

Measurements and Calculations of Fatigue Damage in Ship Structure

Barhoumi Mondher



**Vestfold University College
Faculty of Technology and Maritime Sciences**

Measurements and Calculations of Fatigue Damage in Ship Structure

ABSTRACT

Ship owners' cost and frequency of repairs are a direct result of metal fatigue caused by hull stresses. Therefore, most new advanced vessels have extensive data collection systems to be used for continuous monitoring of engine and hull performance, in order to acquire and record information and then use the information as a basis for making decisions that will improve operational efficiency and safety. Most of the critical wave-induced ship extreme responses and fatigue damage accumulation can be estimated.

The aim of this thesis is to combine measurements and calculations to estimate fatigue damage and extreme loading in hull girder taking into account wave induced vibrations. The wave induced vibrations are often divided into springing when they refer to a resonance phenomenon and whipping when they are transient phenomenon. Both phenomena contribute to crack growth for sensitive details in particular in deck and bottom structure of ships. These vibrations, especially whipping, contribute to extreme loading. These effects are normally neglected in design. The industry view in this is changing.

A large modern container vessel with high bow flare angle and high service speed has been considered. The ship was equipped with a hull monitoring system from a recognized supplier. A valuable data has been collected during the vessel's operation between Asia and Europe. Also model tests have been carried out of this vessel to investigate fatigue and extreme loading. For the full scale measurements, the correlation between stress data and wind data has been investigated. Wind data is easily accessible onboard, while wave data is expensive. Both sources of environmental data have shortcomings. The wave and vibration damage are shown versus heading and Beaufort strength to indicate general trends. The wind data has also been compared to North Atlantic design environment. The model tests have been carried out in head seas for a number of sea states at realistic speeds. The results suggest that the model tests and full

scale measurements show fair comparison, although there are some deviations in the conditions. In both cases the extreme loading defined by IACS URS11 is significantly exceeded when whipping is included, and if whipping may contribute to collapse then proper seamanship is considered necessary in order to limit the extreme loading. From the full scale measurements proper seamanship is also clearly observed. The vibration contribution on the fatigue damage is high, but conservatively estimated from the model tests in head seas. However, it agrees fairly well with the measured data in full scale in head seas. The full scale measurements also cover other headings, and the vibration damage is also observed to be high from head to beam seas, and even present in stern seas.

Selected cases have been assessed to compare the fatigue damage calculated from combination of the Rainflow counting method and the Palmgren-miner rule with damage prediction obtained from frequency fatigue analysis using spectral method. Both methods are in good agreement, when the stresses are moderate. However, when whipping is significant, the results differ and the Rainflow method suggests high fatigue damage estimations even higher than the estimated damage by narrow-band approximation.

PREFACE

This thesis is submitted in partial fulfillment of the requirements for a Master of Science in Maritime Management. It contains work done from January to Mai 2013. My supervisors on the project have been Storhaug G. and Frednes A. T. The thesis has been made solely by the author; based on data analysis and extensive literature study. The thesis includes also a research paper:

Paper: Barhoumi Mother, Storhaug G. “Assessment of whipping and springing on a large container vessel” It will be published in proceeding of the 12th International Symposium on Practical Design of Ships and other Floating Structures, (PRADS 2013). Gyeongnam, Korea.

ACKNOWLEDGEMENTS

The preparation of this thesis would not have been possible without the valuable contribution of many people.

Foremost, I would like to express my sincere gratitude to my supervisor Dr. Gaute Storhaug for the continuous support of my thesis, for his patience, motivation, enthusiasm, and immense knowledge. I also want to thank Mr. Truls Arne Frednes for the beneficial discussions and encouragement.

My next sincere acknowledgment goes to DNV for giving me this opportunity, providing a desk and free access to extensive full scale measurements, giving me the opportunity to meet many good people. I want to thank DNV's staff in the Ship Hydrodynamics and stability and Ship structures and concepts units for beneficial discussions, positive attitude and the excellent working atmosphere.

I want to thank Mr. Lars C. Iversen, leader of Department of Maritime Technology and Innovation in Vestfold University College and all the staff for giving me the opportunity to follow this master program and for all their support.

In addition, I thank the yard, the owner and the master for their assistance. My sincere thanks also go to Light Structures and all the staff for providing all the information regarding the Hull Monitoring system. And special thanks to Dr. Geir Sagvolden for sharing experience and for the fruitful discussions.

Most of all, I am grateful for my family for their support. My special thanks go my mother Jannet for her love and for always believing in me.

Table of Contents

ABSTRACT	1
PREFACE	3
ACKNOWLEDGEMENTS	4
List of tables	8
List of figures	9
Introduction	1
Background	1
Whipping-springing induced:	4
Fatigue assessment of ship structure:	5
Objective of the Thesis	8
Chapter 2	10
Basic Theories and Methods	10
Irregular Stress History:	10
Time Domain Fatigue Analysis.....	11
Frequency Domain Fatigue Analysis	13
Stationary process:	13
Stochastic process:	13
Narrow band approximation:.....	14
Broad band approximation:	14
Rainflow Counting	15
Chapter 3	16
Full Scale Measurements.....	16
The vessel.....	16
Measurement arrangement:	18
Data processing:	19
Sensors and locations	20
Purpose of the full scale measurements.....	22
Chapter 4	24
Trade and Fatigue Loading Overview	24
Trading and Measurement Period:	24
Fatigue Assessment	25
Reversals identification	25
Rainflow spectra.....	25
Fatigue damage accumulation	25

Results from Fatigue Analysis	26
Fatigue analysis for welded details in corrosive environment	28
Fatigue damage for the different voyages	28
Fatigue rate intervals	30
Conclusion.....	31
Chapter 5	32
Fatigue Damage versus Wind Conditions	32
Wind Profile	32
Fatigue Damage versus Wind Headings.....	37
Sector 2.....	39
Sector 1.....	40
Sector 3.....	41
Sector 6.....	42
Sector 5.....	43
Sector 4.....	44
Wind profile for both port and starboard side	45
The effects of voluntary speed reduction	46
Chapter 6	47
Fatigue Spectral Analysis.....	47
General	47
Jiao and Moan Method.....	48
Application of Jiao and Moan spectral method.....	51
Case one:	51
Case two:	53
Linear Springing.....	55
Discussion	56
Chapter 7	58
Extreme Loading.....	58
Chapter 8	63
Summary and Conclusions.....	63
Major Findings and Discussion.....	63
Future Work	67
Appendix A	72
Sensor Names and Locations	72
Amidships between frame 101 and 102	72

At engine room bulkhead between frame 79 and frame 80.....	74
At forward quarter length between frame 131 and frame 132	76
At transverse deck strip:	77
Slamming sensors:.....	78
Appendix B	80
Research Paper	80

List of tables

Table 3. 1: Main particulars for the vessel	17
Table 3. 2: Sensors characteristic, location and definitions.	21
Table 4. 1: Results from fatigue analysis for the different sensors.	27
Table 4. 2: Voyages from the 3rd of June 2009 to the 18th of Mars 2013	29
Table 5. 1: Beaufort scale versus significant wave height ((Pear Drop).....	34
Table 5. 2: Fatigue damage versus wind heading (DMP)	38
Table 5. 3: Fatigue damage versus wind heading (DMS)	38
Table 5. 4: Summarized 5 minutes fatigues rates in different wind headings for both sensors DMP and DMS.....	45
Table 7. 1: Maximum sagging and hogging stress with and without whipping and the IACS wave bending stress rule	61

List of figures

Figure 1 1: 2-node vertical vibration of hull girder.....	2
Figure 1.2 Picture of a longitudinal stiffener in deck in way of the transverse bulkhead in a large blunt ore carrier. The crack originated from the bracket toe termination after one year of operation (Storhaug G. , 2007).....	4
.....	4
Figure 1 3: Structural damage in MSC Napoli after collapse in January 2007. (Cargo Law, 2007).....	4
Figure 1.4: Basic definitions of two-slope S-N curve. (DNV-RP, 2010)	7
Figure 2. 1: Irregular load histories.....	10
Figure 2. 2: Narrow band (left) and broad band (right) loading.	11
Figure 2. 3: Stochastic Process.....	13
Figure 2. 4: Rainflow cycle counting method.	15
Figure 3.1 Photography of the container ship considered in the analysis (Fleet Mon, 2012)	17
Figure 3. 2: A photo of a sensor package glued on a stiffener before coating (Light Structures, Installation manual).....	18
Figure 3. 3: Layout of SENSFIB system with sensors for global and local hull responses, and vertical accelerometers. (Light Structures, Installation manual).....	19
Figure 3. 4: Amidships sensor positions.	22
Figure 4. 1: Sailing area for the vessel.	24
Figure 4. 2: Total and wave 5 minutes fatigue rates for port side deck sensor (DMP).....	27
Figure 4. 3: Total and wave 5 minutes fatigue rates for port side deck sensor (DMS).....	27
Figure 4. 4: Longitude (negative is West, positive is East).....	29
Figure 4. 5: fatigue damage recorded each trip in the DMP and DMS sensors.	30
Figure 4. 6: % of time and % of damage in the different fatigue rate intervals.	31
Figure 5. 1: Measured wind strength distribution versus Argoss.....	33
Figure 5. 2: Average 5 minutes fatigue rates and vibration contribution as function of Bn. ...	35
Figure 5. 3: Wind sectors.	35
Figure 5. 4: Relative wind heading profile.....	36
Figure 5. 5: True wind heading profile	36
Figure 5. 6: % of damage and relative wave/vibration damage versus wind sectors (DMP) ..	37
Figure 5. 7: % of damage and relative wave/vibration damage versus wind sectors (DMS). .	38
Figure 5. 8: % of damage and vibration contribution versus Bn in sector2 (DMP).....	39
Figure 5. 9: Average fatigue rates and average speed versus Bn in sector 2 (DMP).	39
Figure 5. 10: % of damage and vibration contribution versus Bn in sector1 (DMP).....	40
Figure 5. 11: Average fatigue rates and average speed versus Bn in sector 1 (DMP).	40
Figure 5. 12: % of damage and vibration contribution versus Bn in sector 3 (DMP).....	41
Figure 5. 13: Average fatigue rates and average speed versus Bn in sector3 (DMP).	41
Figure 5. 14: % of damage and vibration contribution versus Bn in sector 6 (DMP).....	42
Figure 5. 15: Average fatigue rates and average speed versus Bn in sector6 (DMP).	42
Figure 5. 16: % of damage and vibration contribution versus Bn in sector 5 (DMP).....	43
Figure 5. 17: Average fatigue rates and average speed versus Bn in sector5 (DMP).	43

Figure 5. 18: % of damage and vibration contribution versus Bn in sector 4 (DMP).....	44
Figure 5. 19: Average fatigue rates and average speed versus Bn in sector4 (DMP).....	44
Figure 5. 20: Relative wind headings for port (negative) and starboard (positive).	45
Figure 5. 21: Fatigue rates (DMS), vessel speed, wind heading, Bn, 30th December 2011....	46
Figure 6. 1: The stress spectrum measured for DMP, 17th November 2010 -22:00	48
Figure 6. 2: The position of the vessel in case 2.	52
Figure 6. 3: The estimated hourly fatigue rates in case 1 (DMP).	52
Figure 6. 4: The estimated hourly fatigue rates and the vibration contribution in case 1 (DMP)	53
Figure 6. 5: The estimated hourly fatigue rates in case 1 (DMP).	54
Figure 6. 6: The estimated hourly fatigue rates and the vibration contribution in case 1 (DMP)	55
Figure 6. 7: linear springing: Low and high frequency stress signals, the 2nd December 2011 -23:00.....	56
Figure 7. 1: The maximum 5 minutes hogging (positive) and sagging stress with and without whipping, DMP.	59
Figure 7. 2: The maximum 5 minutes hogging (positive) and sagging stress with and without whipping, DMS.	59
Figure 7. 3: The Measured Stress versus IACS Rule stress from port side sensors.....	61
Figure 7. 4: The Extreme dynamic loading versus wind strength for DMP.	62
Figure 7. 5: The Extreme dynamic loading versus wind headings for DMP.	62

Introduction

There are around 100,000 merchant ships over 100 GT trading internationally. They transport every kind of cargo, with ships registered in over 150 nations. This fleet carries over 90% of the world trade. The average age of the ships is 22 years. Losses from serious incident of a vessel can be huge not only if it refers to the loss of human lives, damaged ship or cargo, but also when the environmental pollution is an issue (IMO, Maritime Knowledge Centre, 2012). Therefore, the shipping industry is one of the most heavily regulated industries, and was amongst the first to adopt widely implemented internationally standards related to design approval, construction and operation including inspection. The regulation of the maritime industry is mainly related to the objective of ensuring safety, security and prevention of pollution from ships. One of the increasing concerns is related to the analysis of fatigue and ultimate strength of ship structures, which is related to maintenance and repair cost as well as safety, illustrated by the development of common structural rules for tankers and bulk carriers by IACS. However, there are still large uncertainties in prediction of fatigue lives, which is mainly caused by uncertainties in the actual environmental and operational profile, as well as uncertainties associated with current calculations procedures used in design, where effects of some phenomena may be neglected at least explicitly e.g. wave induced vibration.

Background

Most often, ocean-going vessels are operating in different loading conditions and nautical zones facing waves which are usually described by stochastic random processes. The interaction between the ship and waves force the hull structure to bend longitudinally upwards and downwards to form hogging and sagging respectively as seen in Figure 1. Sagging and hogging interlace to cause repeated loading and unloading of the hull girder which lead to fatigue damage accumulation. The term of “fatigue” is commonly used in engineering to describe damage due to repeated-load application and effect on the strength and structural integrity of structural member. The exact mechanism of a fatigue failure is complex and is not completely understood. Failure by fatigue is progressive irreversible cracking process, which unless detected and remedied can lead to catastrophic rupture, e.g. the “Alexander L.

Kielland” accident in 1980 in which a semi-submersible platform suffered a fatigue failure of a single brace, leading to structural collapse capsizing and loss of 123 lives (Berge, 1981).

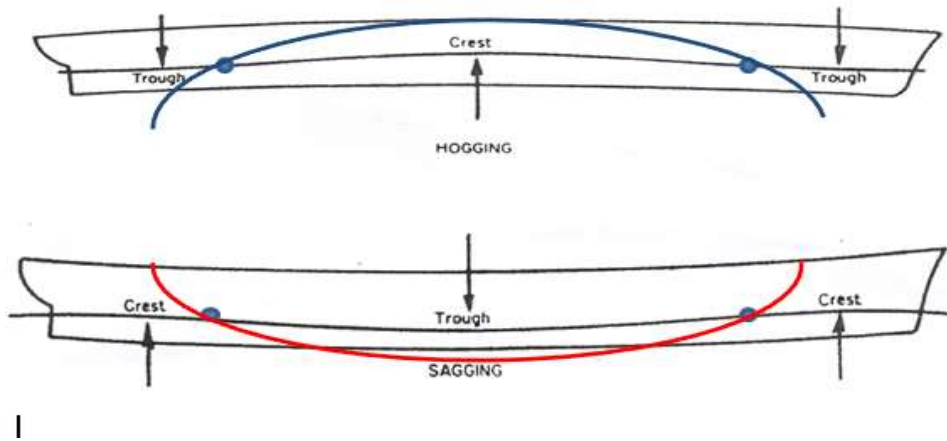


Figure 1 1: 2-node vertical vibration of hull girder

The phenomenon of fatigue was discovered prior to 1850 by observing railway axles failing without apparent cause, and afterwards the understanding of the phenomenon was developed for various types of structures i.e. bridges, aircrafts, offshore platforms and ships. Fatigue damage has been a hot subject in IMO regulation and class rules for several decades, where there are many requirements for fatigue control on ships. The aim of the control is to ensure that all parts of the hull structure subjected to fatigue (dynamic) loading have adequate fatigue life. ASTM (American Society for Testing and Materials) defines the fatigue life as the number of stress cycles that a specimen sustains before failure occurs, (ASTM 1997). Fatigue failure can take place when the maximum stress value is less than the ultimate tensile strength or possibly even below the yield stress limit.

Although ship structural member are designed to survive 20 years or more, fatigue crack damage still occurs, often starting very early in the ship’s life, see figure 1.2.

Further, the structural analysis includes yielding strength, buckling strength and ultimate strength. The structure deforms plastically if the tensile stresses exceed the yielding point of the material, and if it increase even higher to reach the ultimate tensile strength the ship may collapse starting from local failure. In some cases a high compressive stress lead to structural buckling and further to collapse, e.g. the collapse of MSC Napoli due to overloading from high wave bending, (Storhaug G. , THE 4400TEU CONTAINER VESSEL MSC NAPOLI BROKE IT BACK, BUT DID WHIPPING CONTRIBUTE?, 2009). The

collapsed MSC Napoli is seen in figure 1.3. This shows the importance of the assessment of the design extreme responses of the ship structures which shouldn't exceed the ultimate strength of the material, and the critical buckling stresses in order to keep the integrity and safety of the hull structure. Other reasons of ship accidents may be navigational errors, such as grounding, collision etc.

Currently, the conventional wave loading is the only effect considered explicitly in fatigue assessment of ships, all wave loads encountered by the ship in e.g. North Atlantic(NA)/World Wide(WW) trade are taken into account normally based on linear hydrodynamic theory assuming that the hull girder to be rigid.

In reality the hull girder is however flexible and normally the vertical 2-node vibration mode in the lowest hull girder frequency with natural period about 2s, see Figure 1. Wave and slamming excite continuously the vibration as springing or whipping. And full scale measurements have shown stress components to follow the 2-node vibration and to show both transient and more continuous variations. (Okada, Takeda, & <aeda, 2006). In structural design of ships these high frequency stress amplitudes are in general not accounted because they are considered much smaller than those in the wave frequency region. However, by the increase of the arctic operation and also the opening of the new Panama channel 2014, more container vessels will be introduced in harsher environment. Especially with the increasing length of these ships with reduced relative stiffness, some concern has been expressed on the importance of these high frequency stress components both with respect to extreme loading and also to their contribution to the expected fatigue damage, (Storhaug, Moe, & Piedras Lopes, 2007). The fatigue contribution from wave induced vibration is reported to be comparable to the conventional wave loading. And whipping contribution may also lead to a significant increase of the predicted extreme responses of the ship structures, (Storhaug, Pettersen, Oma, & Blomberg, 2012).



Figure 1 2: Picture of a longitudinal stiffener in deck in way of the transverse bulkhead in a large blunt ore carrier. The crack originated from the bracket toe termination after one year of operation (Storhaug G. , 2007).

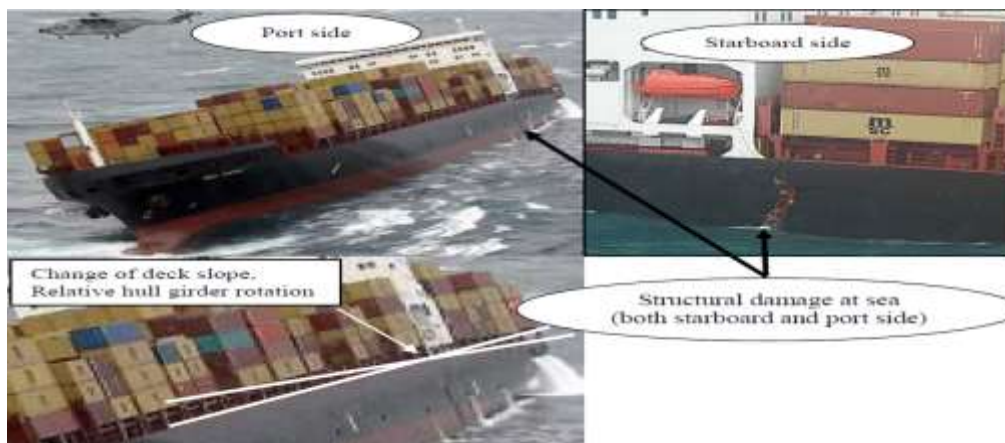


Figure 1 3: Structural damage in MSC Napoli after collapse in January 2007. (Cargo Law, 2007)

Whipping-springing induced:

Wave-induced hull girder vibrations are normally described by the terms springing and whipping. Sometimes the term swinging is used for vibrations in the horizontal plane (lateral vibrations), while springing and whipping are then reserved for vertical vibrations. Springing is resonant vibrations that sustain over a certain period (steady state phenomenon). It is due to wave forces that oscillate with the same frequency as one of the natural frequencies of the hull girder. Usually the lowest frequency (2-node mode for mono-hull, twisting mode for catamaran) are more critical. Torsional vibration may also occur for ships

with large deck opening, such as the container vessel which will be considered in this thesis. High forward speed and low natural frequency tend to increase both springing and whipping, (Hermundstad, 2007).

Whipping is transient hull girder vibrations due to wave-loads that increase rapidly, normally an impact of loads arising from bottom slamming or bow flare slamming. 2-node and 3-node vertical vibration modes are the most important.

In some wave conditions a ship may experience slamming loads for almost every wave encounter. With low damping, this gives rise to continuous hull girder vibrations of varying amplitude. This illustrates that there is not always a clear dividing line between whipping and springing.

The highest hull girder responses are often associated with whipping events, hence whipping may contribute to increase risk of collapse of the whole hull girder (e.g. MSC Napoli 2007). Springing may also contribute to extreme responses for some ships but it is normally more important for fatigue. In 1999 DNV started again (first time was in the 1960s) to assess the consequence of vibration on blunt ships and results from full scale measurements model tests show that the fatigue contribution from wave induced vibrations is comparable to conventional wave loading (Storhaug et al. 2003) . Following up the findings on blunt ships also container vessels have been instrumented, 4400TEU in 2002 and 2800TEU in 2007, where result showed that vibration contributes to about 29% of the fatigue damage for the first vessel and 26% for the second, (Storhaug 2012). Model tests have been also carried out for an 8600TEU container vessel in head seas, and showed that vibration damage is dominating source of fatigue, with about 86% amidships but the damping was a bit low, Storhaug (2010). In 2009, an 8600 container vessel was instrumented, and this is considered in this thesis.

Fatigue assessment of ship structure:

Fatigue is a process of cycle by cycle accumulation of damage in material subjected to cyclic loading, and loads are not large enough to cause immediate failure, while after certain number of load fluctuations a crack may be detected and start to grow faster until it is arrested or to final fracture.

The most important load effect parameter in fatigue is the fluctuating component of stress or strain, referred to stress range or strain range, which is defined as the difference between a load peak and the subsequent valley. For ships, most often the stress range fall within the material elastic range during the service period, and the failure of the ship structures usually

requires approximately more than 10^5 cycles, commonly referred to as high cycle fatigue. The high cycle fatigue estimation is based on the stress range.

In addition to the high cycle fatigue induced by waves, the fatigue strength could be effected by the repeated yielding as occurring during the cargo – ballast loading cycles, known as low cycle fatigue normally below 10^5 cycles. In this range the structural materials undergo cyclic plasticity and the stress range is no longer a good parameter, then the strain range is used for modeling the low cycle fatigue. For ships fatigue stresses are mainly in the high cycle range and the low cycle range is generally not or briefly defined in relevant design. Hence, the strain based low cycle fatigue analysis is not covered in this thesis

For high cycle fatigue analysis, fatigue data is normally presented in a stress-life diagram, S-N curve, (also known as Wöhler curve). Stress range ΔS versus number of cycles to failure N is plotted on log-linear dependence, see Eq. 1.1, (DNV, 2010)

$$\log(N) = a - m \cdot \log(\Delta S) + e \quad (1.1)$$

Where $a > 0$ and $m > 1$ depend on the material properties, structural details and the stress ratio R . While e is random error. Those parameters are derived from tests on samples of the material to be characterized, where a regular sinusoidal stress is applied by a testing machine which counts the number of cycles to failure. The tests are often called coupons and the process called coupon testing. Each coupon generates a point on the plot. At low stress ranges specimens may have infinite life i.e. fatigue life significantly longer than reasonable testing time. Therefore, a run-out life is defined somewhere between $5 \cdot 10^5$ - 10^7 cycles. The S-N curves are based on the mean minus two standard-deviations curves for relevant experimental data, S-N are thus associated with 97.6% probability of survival.

In marine ships the S-N curves with a single slope and two slopes for welded joints in air are mostly used. There is also S-N curve for corrosive environment. The basic definitions of two-slope S-N curve is illustrated in Figure 1.4. Parameters of the relevant S-N curves are usually given in ship classification rules for different ship details (material and structure types). For example, several S-N curves used in the (DNV-CN 30.7 2010).

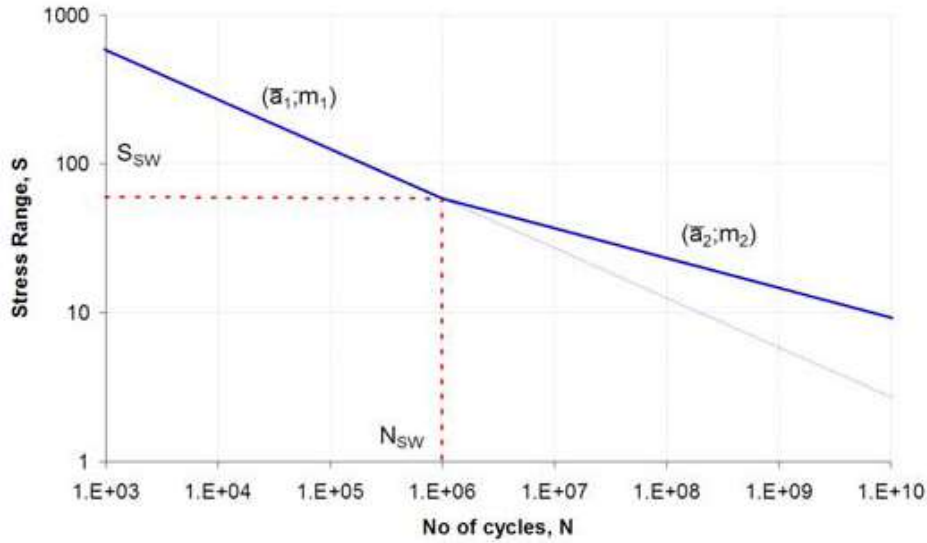


Figure 1 4: Basic definitions of two-slope S-N curve. (DNV-RP, 2010)

The Ship structural components are exposed to a complex, often random, sequence of loads when ships are sailing. In order to evaluate the safety level of the components, the stress cycles of the random loads are first extracted using a certain technique. The fatigue life under varying loading is calculated based on the S-N fatigue approach under the assumption of linear cumulative damage e.g. Palmgren-Miner’s rule, (Palmgren (1924) and Miner (1945)), other non-linear fatigue accumulation laws may be used, (Fatemi 1998) . The Palmgren-Miner’s rule is most accepted because it is simple form for applications. The total damage the structure is experiencing may be expressed as the accumulated damage from each load cycle at different stress levels, independent of the sequence in which the stress cycles occur, Eq. 1.2

$$D = \frac{1}{a} \sum_{i=1}^k n_i \cdot (\Delta S_i)^m \quad (1.2)$$

Where D is the accumulated fatigue damage, which is assumed to be 1 for design purposes but experimentally is found between 0.7 and 2.2 when the failure occurs, a and m are the S-N parameters, k is the number of stress blocks, n_i is the number of stress cycles in stress block i .

In ship design the fatigue life prediction is based on the distribution of stress ranges ΔS and the total number of stress cycles N that are usually described by some empirical functions for different type of ships at different locations in the rules, such as (IACS, 2006) or the (DNV, 2010). The stress range is often divided into k segments from 0 to the maximum stress range

ΔS_{max} i.e. $0 \leq \Delta S_1 \leq \dots \leq \Delta S_i \leq \dots \leq \Delta S_{max}$ and the accumulated damage is calculated based on eq. 1.3.

$$D = \frac{N}{a} \sum_{i=1}^k P_i \cdot (\Delta S_i)^m \quad (1.3)$$

Where P_i is the probability of the stress ranges that have occurred in i^{th} segment. The stress cycles are defined by a certain counting method. The Rainflow counting method, proposed by (Matsuishi & Endo, 1968) is the most frequently used for fatigue life prediction. Other methods were proposed in literature such as level crossing counting, Peak counting, min-max counting and other procedures. More details about the counting methods are described in (ASTM 1997). The empirical distribution of the stress is not available for new type of vessels. Thus, some more sophisticated methods may be used for fatigue analysis. The ship operation period is assumed to be composed of series of stationary sea states, which describe the general condition of the wave elevation surface. The sea state is usually assessed by some instruments like buoys, wave radars, or satellites, to define the statistical parameters of the wave, significant wave high H_z , wave period T_p and the power spectrum. The ship responses at each sea state can be computed by numerical analysis or measured by strain sensors. Further, the fatigue damage accumulation at different sea states can be estimated either by time-domain fatigue analysis or by spectral fatigue analysis in frequency domain. Different methods and theories used in fatigue analysis are presented in chapter 2.

It should be noted that the variable amplitude loading sequence has a significant influence on fatigue accumulations; see (Barsom, 1976), (Van Paegpegem & Degrieck, 2002), and (Taheri, Trask, & Pegg, 2003). It is also reported that the effect of mean stress on fatigue damage has been widely studied in literature, for example (Goodman, 1919), (Smith, Watson, & Topper, 1970) Dowling (2004), and (Johannesson, Svensson, & De Mare, 2005) etc. However, in this research, both effects have been omitted for the current fatigue analysis, assuming the whole load cycles to occur in tension. This is a fair assumption since the focus is on sensors located on deck of a container ship which is a “hogging” vessel with tension in deck.

Objective of the Thesis

The objective of the thesis is to assess fatigue and extreme loading on ship structure considering both the conventional wave responses and the high frequency responses such as whipping/springing. The thesis study how the wave induced vibrations affect the fatigue

damage accumulation based on full scale measurements. The fatigue loading and the effect of the vibration are evaluated and presented as function of the different wind heading and Beaufort strength. The effect of whipping on the maximum loading is assessed, and the total dynamic stress is compared to the IACS rule wave bending stress.

The background and motivation has previously been covered in this chapter. The thesis contains 7 more chapters and they are arranged as follows:

- Chapter 2 presents some basic theories and models in order to better understand the detailed contents of the thesis.
- Chapter 3 explains the concept and the purpose of full scale measurements. The measurements arrangements and overview of the considered sensors and their locations are presented in this chapter. The main particulars and characteristics of the considered vessel are also introduced.
- In chapter 4, a summary of the trading routes and the measurements period are presented. A brief introduction to the fatigue assessment is given and the fatigue loading in different voyages and different fatigue rate intervals are studied.
- In chapter 5, the wind data is assessed and compared to North Atlantic design environment, and the wind heading profile is established. The fatigue damage is studied for the different wind headings and the effect of wave induced vibration is evaluated.
- In chapter 6, a spectral method is used for fatigue analysis and compared to results from traditional procedure, which correspond to the combination of S-N curves of welded joints, the Rainflow counting and the cumulative damage law.
- Chapter 7 study the maximum dynamic stresses in 3 different sections of the deck, aft amidships and forward. The maximum dynamic stresses are compared to the IACS rule wave bending stress values. The importance whipping contribution in increasing the maximum stresses are investigated as function of wind headings and Bn strength.
- In Chapter 8, summary of the thesis, conclusions and major findings are given followed by some suggestions for future work.

Basic Theories and Methods

Irregular Stress History:

During operation, the ship structures will experience stresses that vary with time, often in a very complicated manner. These stress histories are generally the results of an irregular load history and the dynamic response of the hull structure. In figure 2.1 is an example of irregular load history.

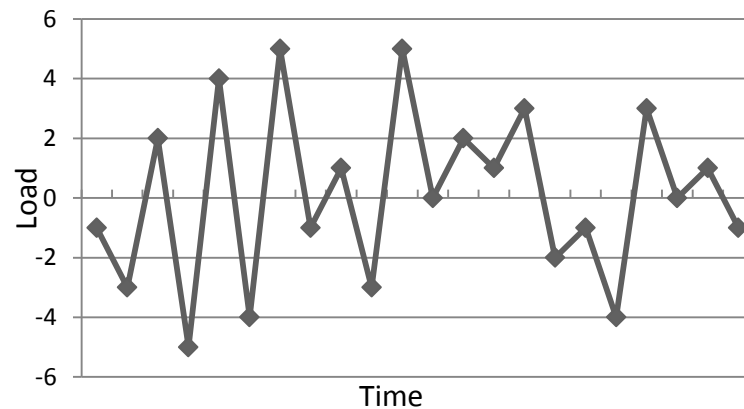


Figure 2. 1: Irregular load histories.

The most important concepts related to irregular load histories are the following:

- Reversal/Turning point: occurs where the first derivative of the load history changes sign, “Peak” when the sign change from positive to negative and “Valley/trough” when the sign changes from negative to positive.
- Stress range is the algebraic difference between successive valley and peak
- Mean crossing: or zero-crossing, is the number of times that the load history crosses the mean load level, normally crossing with positive slopes are counted (up-crossing).
- Irregularity factor: is a factor that measure the regularity or the bandwidth of the stress signal, defined as the ratio of the mean up-crossing to the number of peaks or Valleys in a given load history. (Almar Næss, 1985)

With narrow band time series as shown in Figure 2.2 individual stress cycles can easily be identified and counted, e.g. by counting one stress cycle for each zero up-crossing and take the stress range as the difference between the peak and the valley values.

In broad band time series, where large cycles are interspersed with small cycles with varying mean level, left plot in Figure 2.2, the question of what is meant by a cycle and the corresponding stress range becomes less evident. It is therefore necessary to use a cycle counting method that in an unambiguous way breaks the stress history down into individual cycles which can be summed up into a stress range distribution.

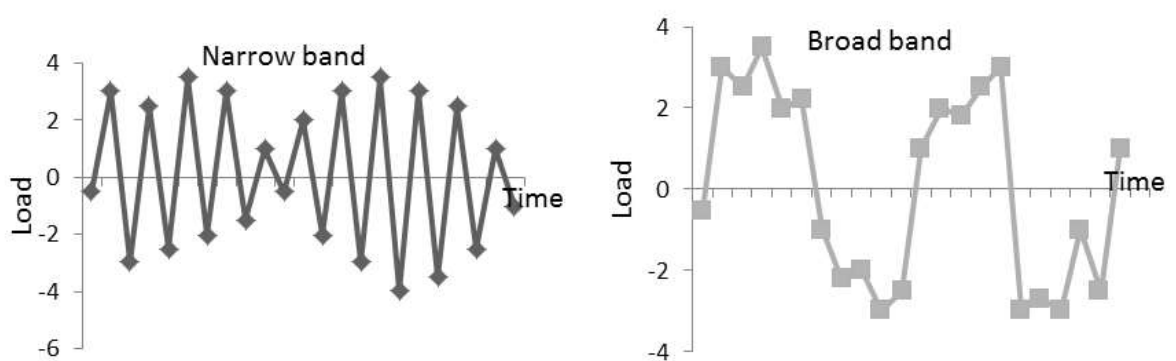


Figure 2. 2: Narrow band (left) and broad band (right) loading.

Several methods have been proposed for general cycle counting of broad band processes, generally leading to different results in terms of accumulated fatigue damage. Cycle counting procedures that give the most correct physical representation of the fatigue process are therefore often preferred.

For narrow band time series the choice of counting method seems less critical, and most generally accepted methods lead to quite similar results. For high cycle fatigue the most frequently used cycle counting methods are the Reservoir Counting Method and the Rainflow Counting Method. As the Rainflow Counting Method is used in his research, the following will focus on the details of this method. Several other counting methods exist, and they are reviewed in (Schijve, 1963).

Time Domain Fatigue Analysis

The starting point for any fatigue analysis is the response of the structure or the structural detail. In time domain fatigue analysis, the stress history is usually available, by

measurements or calculations, and the damage accumulation can be estimated e.g. by Palmore-Miner's rule, eq. (1.2). The stress ranges in eq. 1.2 are counted from the stress time history by a cycle counting method. There are a number of cycle-counting algorithms for such applications, the Rainflow method is the most popular and it is believed to give the most "accurate" fatigue life prediction, (Dowling, 2004) and (Watson & Dabell, 1975). The Rainflow counting method is developed on the hysteretic properties of material, where the cyclic stress-strain curves form hysteretic loops. The local maxima are represented by tops of the loops, while local minima by bottoms of the loops. The Rainflow method is to identify the local minimum which should be paired with a local maximum to form a hysteretic loop. The Rainflow method is explained further in the next section 2.4. (Rychlik, 1993) propose another approach for the stress cycles counting, which is the crossing counting method. This method pairs the Peaks and Valleys into cycles giving the priority to large cycles in the stress. The crossing counting method leads to the maximum estimation of accumulated fatigue damage. Hence, this method can be considered as the upper bound for the Rainflow damage. Another method of the time domain fatigue analysis has been proposed by (Gotoh, Matsuda, & Kitamura, 2012). It is a numerical simulation for fatigue crack propagation which use new material parameter RPG (Re-tensile Plastic zone Generating) load criterion based on advanced fracture mechanics approach to enable the extraction of the effective loading history. The identification method of the RPG load is explained in reference (Toyosada, Yamaguchi, Niwa, Takenaka, Kajumoto, & Yajima, 1991). In (Gotoh, Matsuda, & Kitamura, 2012) a new extraction algorithm of the effective loading histories has been proposed for fatigue crack propagation under superposed loading histories. The validity of this method has been confirmed by measurements. And the comparison with the Rainflow and S-N curves approach under superposed loading conditions show that the Rainflow method overestimates the fatigue damage. This was mainly due to the delay in fatigue crack growth when small stress range cycles followed a large stress cycle, e.g. the case of whipping.

For the fatigue design of ship structures, all possible sea conditions in the wave scatter diagram (DNV, April, 2007.) should be considered. The computation of stresses for the ship at all different sea states is extremely time-consuming. Therefore, an alternative approach is to use the spectral fatigue analysis, where ship stresses are assumed to be Gaussian.

Frequency Domain Fatigue Analysis

Stationary process:

A process is said to be stationary if the statistical properties do not vary with time. Many processes may be considered stationary provided the time period considered is short enough. This is e.g. true for the sea surface elevation, which normally is considered stationary within time intervals of 20 minutes to 6 hours (DNV, .April, 2007.)

Stochastic process:

In practical design work the stress history is often found to be irregular and in some cases also random. The popularity of such processes stems primarily from two essential properties. First, a Gaussian process is completely determined by its mean and covariance functions. This property facilitates model fitting as only the first- and second-order spectral moments of the process require specification. Second, solving the prediction problem is relatively straightforward. The best predictor of a Gaussian process at an unobserved location is a linear function of the observed values and, in many cases, these functions can be computed rather quickly using recursive formulas. The stress range history can therefore be considered a stochastic process, where we describe the process by its statistical properties, i.e. mean value and standard deviation.

The energy spectrum of the process $S(\omega)$ can be found directly from the stress process $X(t)$ using Fast Fourier Transform (FFT). When performing FFT on a time signal we transform the process given by $X(t)$ in the time domain into its equivalent representation in the frequency domain $X(\omega)$, from which we can derive the energy spectrum $S(\omega)$. It is normal to distinguish between narrow band processes and broad band processes, and to characterize a process with its energy spectrum $S(\omega)$ as shown in Figure 2.3.

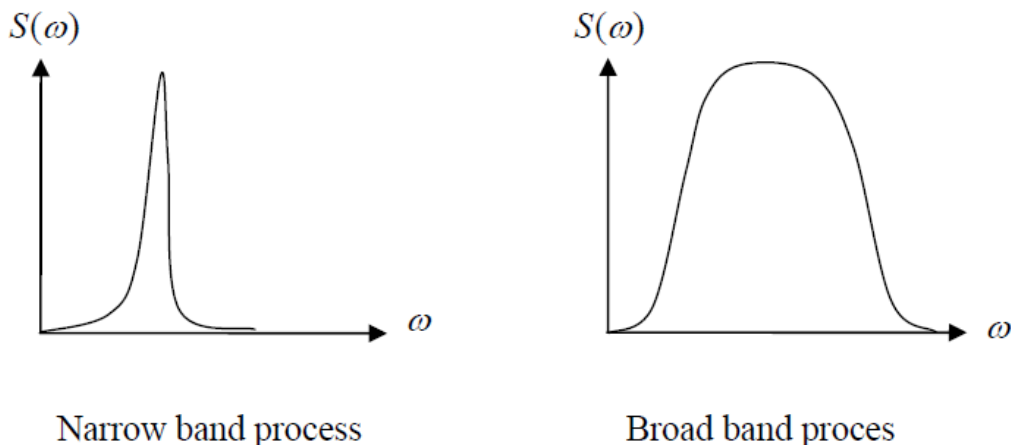


Figure 2. 3: Stochastic Process.

Narrow band approximation:

The narrow band approximation (NBA) has been proposed by (Bendat, 1964) to approximate fatigue damage for a narrow-band process by the corresponding up-crossing spectrum. This method is well applicable for the symmetric loads when the stress history can be approximated by narrow banded Gaussian process. Therefore, the formula of fatigue damage is simply expressed by the first and the second-order spectral moments of the Gaussian load. For broad-band processes, the NBA may lead to a severe overestimation of the expected Rainflow damage. Hence, several effective methods have been proposed for the wide banded-Gaussian process.

Broad band approximation:

To reduce the conservatism and to find more accurate fatigue damage a simple way is to split the spectral into two different components. This method is applicable for the bimodal spectrum where the spectrum can be split into Low-Frequency (LF) part, which is the slowly varying loads and the High-Frequency (HF) part, which is the oscillations superimposed around the LF components. The LF part includes all the large stress cycles and the HF part includes the smaller reversals. The narrow band approximation is still used to estimate the damage from both LF and HF components. The total damage is the summation of contributed fatigue of the two components. This method has been proposed by (Sakai et al.1995), and further investigated recently in (Olagnon & Guédé, 2008). However, in (Benasciutti & Tovo, 2007) states that this approach may give non-conservative predictions when the HF part contains too much energy.

Another theoretical model is introduced by (Jiao et al.1990) where an interaction term between LF and HF components is proposed. The model uses an envelope process which is approximated as the sum of the slow process LF and the C-L envelope (Cramer and Leadbetter) of the faster process HF, (Van Dyk, 1981). This method has been investigated in (Gao & Moan, 2007) and has provided quite accurate results especially for large LF contributions. This method is used in Chapter 6, spectral fatigue analysis.

Rainflow Counting

Rainflow cycle counting method has initially been proposed by (Matsuishi & Endo, 1968) to count the cycles or the half cycles of strain-time signals. It is also known as the pagoda-roof method. Later on, the Rainflow counting method becomes standardized as several counting algorithms published in ASTM (2005). The method is based on the following principle: While placing the graphical display of the stress history vertical, it is considered as a stack of roofs. Rain is assumed to flow from each roof, see figure 2.3. Water flows downward following some general rules described below (Almar Næss, 1985):

- The Rainflow starts at a trough (or peak), and flows down the pagoda roofs until it reaches a more negative trough (or a more positive peak) than the trough (or peak), from which the Rainflow starts.
- The rainflow stops when it encounters another Rainflow which flows down from the previous roof.
- The Rainflow terminated at the end of the time history.
- New Rainflow will not start until the current Rainflow is stopped.
- Each Rainflow path forms a half-cycle, and the horizontal length of the path is considered as that stress range.
- Trough-generated half-cycle will match a peak-generated half-cycle to form a whole cycle.

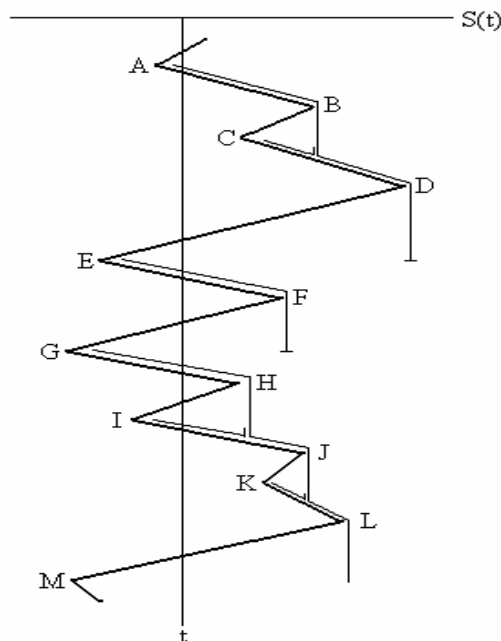


Figure 2. 4: Rainflow cycle counting method.

Full Scale Measurements

Full scale measurements refer to a system installed on board ships or offshore platforms to provide real time quantitative data about motions, sea states, stresses, fatigue loading etc. The system uses sensors to record data, which is processed stored and sent to further assessment onshore. It can be related to hull structure, engines, shafts, comfort, motions or environmental data.

In the current thesis full scale measurement from an 8600TEU modern design Post Panamax container vessel has been considered. The vessel has extreme high bow flare angle (about 63°) and high service speed.

The vessel

The 8600TEU seen in Figure 3.1 was built in 2009 to the DNV Class with the notation “1A1 Container Carrier E0 CSA-2 NAUTICUS (Newbuilding), which implies direct hydrodynamic and structural analysis during the design phase. CSA-2 notation implies reduced risk of fatigue cracking compared to minimum industry standard for ships. This Post-Panamax vessel has been designed for 40 years target life in World Wide trade (WW). More characteristics of the ship are given in table 3.1



Figure 3. 1: Photography of the container ship considered in the analysis

Table 3. 1:

Main particulars for the vessel

Main characteristics	Value
Length overall, L_{OA}	339.6 m
Length between per. L_{PP}	322.6 m
Rule length, L	318.41 m
Breadth, B	45.6 m
Depth, D	24.6 m
Draft design, T	13 m
Draft scantlings, T	14.5 m
Deadweight at design, dwt.	95810 tones
Service speed at design draft, V	28.6 knots
Container capacity,	8562 TEU
Block coefficient, C_B	0.621 [-]
Neutral axis above base line, Z_n	11.26 m

Measurement arrangement:

The vessel was equipped by SENSFIB Hull Stress Monitoring System. It is more comprehensive with more number of sensors than a standard system. The system is supplied by Light Structure AS (LS) and was installed by the yard and the maker.

The system consists of the following main components:

- Fiber optic strain sensors measuring strain and local temperature. An example of installed optical sensor is shown in Figure 3.2.
- Accelerometers measuring vertical acceleration in the bow.
- Fiber optic distribution network to transfer signals from sensors to measurement unit.
- Fiber Bragg grating analyzer (FBG analyzer) measures the optical wavelength signal from the sensors and converts it to a digital signal. It offers the fastest measurement rate compared to other systems.
- Computer receives digital sensor signals from the FBG Analyzer and from other systems such as the navigation system. The signals are fed into the HullInfo processing system.
- Wheel house display: the HullInfo user interface is displayed on thin film transistor (TFT) monitor in the wheel house that contains: TFT monitor, keyboard, mouse, NMEA interface to other systems (loading computer, GPS, Wind sensor), NMEA output to Voyage data recorder (VDR), alarm control system and other systems.
- Uninterruptible power supply (UPS) provides stable power to the system and automatically switches to internal battery power in case of a power failure.

The layout of the SENSFIB system is illustrated in Figure 3.3



Figure 3. 2: A photo of a sensor package glued on a stiffener before coating (Light Structures, Installation manual)

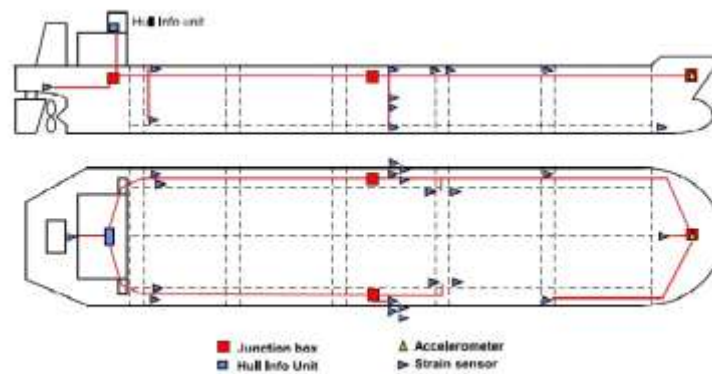


Figure 3. 3: Layout of SENSFIB system with sensors for global and local hull responses, and vertical accelerometers. (Light Structures, Installation manual)

The system measures the strain in several sensor positions on the hull, and it receives data from other ship systems, navigation data and the loading computer.

The choice of the optical sensor was to give better performance of the system. Some advantages of the fiber optic system compared to the conventional strain sensor systems are:

- Signal transferred with low noise and “cross talk”. No interference between light in fiber optic cables and other signals in electrical cables.
- Robust with respect to various chemicals.
- Multiplexing: In a single glass fiber several signals from different sensors can be transferred.
- Explosion safe technology. The power transmitted in cables is very low and failures in cables or sensors will not give rise to sparks.
- Light weight and flexibility on locating the sensors. In most cases sensor are placed on longitudinal stiffeners. Close the hot spots. This give a better representation of the hull girder stress than a placement above deck on hull plates.

Data processing:

The digitized information (wavelength) received from the measurement unit is converted to true wavelength. Then, it is converted to stress and corrected for temperature effects. The obtained data is filtered to obtain different types of time series:

- Raw: unfiltered data (RAW).

- Dynamic: Responses with temperature/still water removed (above 0.01Hz) (DYN)
The dynamic response data may be combined with static values from loading computer (DLC).
- Wave: wave frequency ship responses (from 0.01Hz to 0.3Hz) (WAV).
- Vibration: only vibration responses (above 0.45Hz) (VIB).

Other data from auxiliary sources are received and converted into an internal data stream format.

All data streams are processed by the software for several purposes, such as:

- Slamming event detections and warning of loading exceeding 80 and 100% of rule loading, in term of vertical bending stress, dynamic and static.
- Turning point (reversals) detection which are processed using Rainflow method to produce the response spectra.
- Calculation of bending moments in specified cross sections along the hull.
- Statistic process to produce statistical data and store it in statistical files for 5 minutes and 30 minutes intervals (stat5 and stat30). These statistical data have mainly been used in this thesis.
- Fatigue analysis based on the Rainflow spectra and pre-entered parameters of stress concentration factor (SCF), the S-N curve and target life of the structure. This is stated in the configuration file.

Sensors and locations

The system contains 20 strains sensors for global and local hull responses and bow accelerometers. The sensors are placed on stiffeners at different locations in the vessel and they are distributed as follows:

- 8 sensors at amidships cross-section (4 port and 4 starboard),
- 4 sensors at the engine room bulkhead (2 port and 2 starboard),
- 2 sensors at forward quarter length (1 port and 1 starboard),
- 4 sensors at transverse deck strip (2 port and 2 starboard),
- 2 slamming sensors.

Figure 3.4 shows how sensors are distributed in amidships section. More details about sensors and locations are explained in the Appendix A.

In this thesis the focus will be mainly on global response sensors shown in Table 3.2.

Table 3. 2:

Sensors characteristic, location and definitions.

Sensor	DAP/DAS	DMP/DMS	DFP/DFS
Location	L/4	L/2	3L/4
Y[m] [*]	±21.94	±22.29	±22.10
Z[m] ^{**}	24.42	24.34	24.35
Zv[m ³]	50.2	56.8	41.3
Zh[m ³]	±81.0	±104.2	±53.5
Definition	Deck midship Port/ Starboard	Deck Aft Port/ Starboard	Deck Forward Port/ Starboard

* Distance from central line. ** Distance from base line

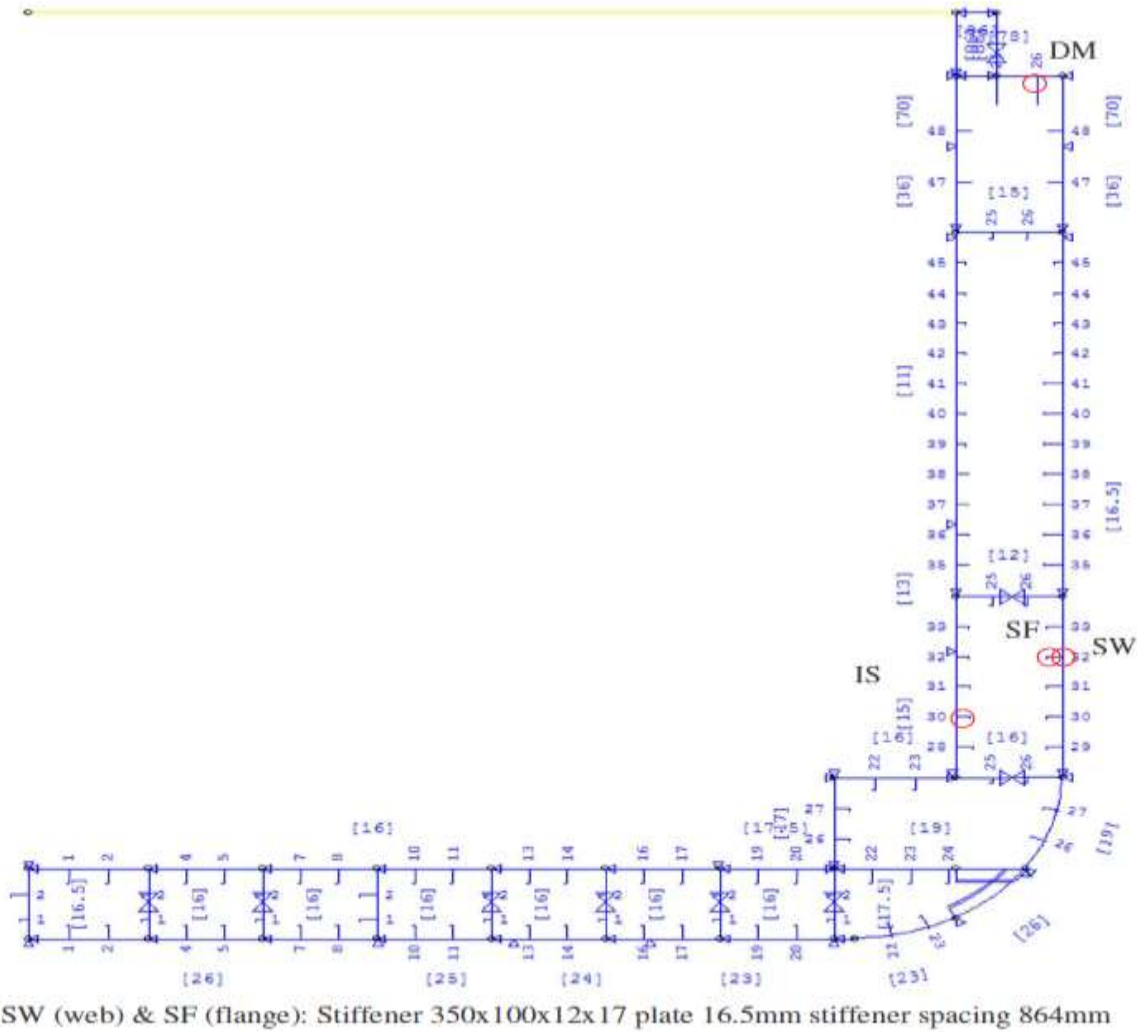


Figure 3. 4: Amidships sensor positions.

Purpose of the full scale measurements

Full scale measurements are used basically to:

- Provide real-time information of the hull stress and fatigue accumulation at sea or during loading/unloading operations.
- Determine the importance of the additional fatigue damage caused by wave induced hull girder vibrations.
- Determine the importance of the wave induced vibrations on the “extreme” loading.
- Determine the relative importance of different stress components, e.g. the warping stress in the deck corner for the purpose of fatigue assessment.

- Measure and evaluate extreme events with respect to whipping (bow damage), parametric roll (loss of containers), if the vessel should encounter such unwanted events.
- Measure side shell fatigue loading, and separate global loads and local bending due to hydrodynamic pressure.
- Indicate the importance of routing in different trades, and the operational profile (heading and speed) compared to design assumptions.
- Define basis for acceptance criteria in design and operation
Compare various calculations with measurements to provide input to future design specifications and rule development.
- Provide documentation for inspiration and motivation for further research and development/modification of numerical codes.
- Provide data to Universities, who do not have the necessary resources or experience to carry out such measurements.
- Full scale measurements can be compared to model tests, which can be carried out in a more controlled wave environment. The latter is suitable for comparison with numerical tools, but may not be representative for the actual encountered sea states.
- Reveal physics which are not considered in design.
- Confirm conditions on board as input to maintenance strategies.
- Ensure safe and cost effective operation.

Trade and Fatigue Loading Overview

Trading and Measurement Period:

The data considered was collected from 03th of June 2009 to 18th of Mars 2013 on board the 8600TEU vessel which was operating between Asia and Europe i.e. east and south China Seas, Indonesian sea, Gulf of Aden, Red sea, Mediterranean Sea, Bay of Biscay and North Sea. The main visited port are Hamburg, Rotterdam, Singapore, Shanghai, Hong Kong and Busan. The position plot in Figure 4.1 show that the vessel was trading mainly in East Asia to Europe trade with only 15% of the time spent in North Atlantic (NA), which is defined as north of 40° N in the Atlantic Ocean. It is observed that there is no significant routing to avoid storms, this differs a lot from North Atlantic crossings, (Storhaug G. , 2012). During the considered period, the stored statistical data contains 390623 five minutes records, i.e. 3.7 years of effective measurements. It should be noted that the hull monitoring (HMON) system was running 98% of the time, it was off for some short periods e.g. from the 14th of August 2010 to 28th of August 2010.

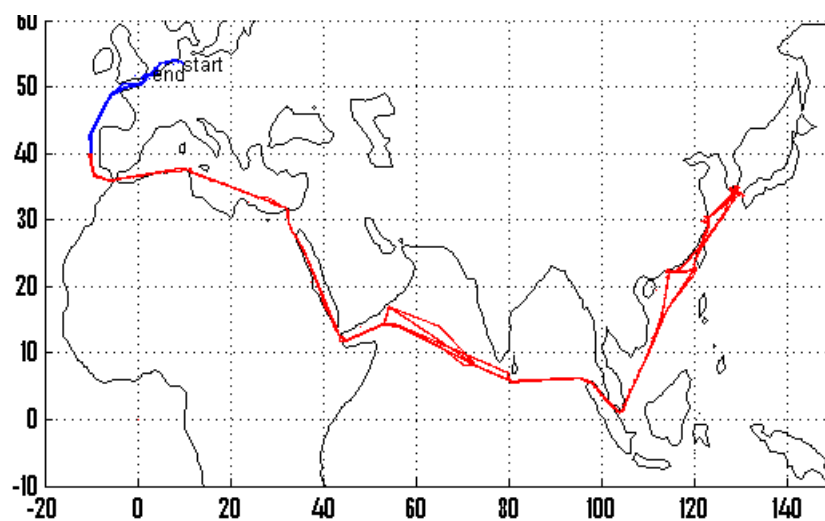


Figure 4.1: Sailing area for the vessel.

Fatigue Assessment

Fatigue analysis is based on analyzing data to carry out the following steps: Identifying the reversals of the stress time series, establishing Rainflow spectra and estimating the fatigue accumulation damage.

Reversals identification

Reversals are identified when the local derivative of the time series change sign. “Peak” is identified when sign change from positive to negative while “valley” is identified when sign change from negative to positive. Cycles less than a threshold level are removed.

Rainflow spectra

The Rainflow counting procedure is made according to ASTM standard (ASTM, 2005). It counts the number of half cycles of a given range (bin). The spectra are divided into a number of evenly sized bins, where each bin represents a given range interval. The spectra are made at regular time intervals e.g. 5mins, 30mins and one hour, for direct calculation of fatigue accumulation rates, or for storage to enable the reanalysis of the fatigue development of the vessel using different parameters than pre-set in the configuration of the system, i.e. S-N curve, stress concentration factor (SCF) etc.

Fatigue damage accumulation

The fatigue loading has been calculated based on the Rainflow spectra. The total damage is estimated from the measured time series with wave induced vibrations, noise and low frequency cycles are removed. The wave damage is estimated from the measured time series filtered to remove also the wave induced vibrations. The vibration damage is estimated as the difference between the total and the wave damage.

The damage for each sensor is calculated according to Miner-Palmgren rule.

$$D = \sum_{i=0}^n \frac{n_i}{N(\sigma_i)}$$

Where D is the damage parameter starting from 0 at the beginning of the lifetime of the vessel, and grow. When it exceeds 1 then the design budget have been spent, n_i is the number of observed full cycles for rainflow bin number i and $N(\sigma_i)$ is the total number of cycles of size σ_i to failure, as given by the SN curve.

The S-N curve used in the configuration is two slope S-N curve for welded details in air. The stress concentration factor (SCF) of 2 is used for the considered sensors. This process is made for the total stress time series, which include wave induced vibration (DYN) and this gives the total fatigue damage. Thereafter the process is made for the stress time series which is filtered to remove contribution of stresses above 0.3Hz (WAV), which give the wave damage. Finally, the vibration damage is the difference between the total and the wave fatigue damage. For observation purposes, the accumulated damage during an observation interval of 5 minutes/30 minutes is scaled by the target lifetime of the vessel to obtain fatigue rates. Five minutes fatigue rate is defined as five minutes fatigue damage divided by the five minutes budget damage, which depends of the target design life. The target life was set to 40 years in this case (error in reference (Heggelund, Storhaug, & Choi, 2011) states 20 years, which led to wrong understanding of the maximum fatigue rates). The 5 minutes budget fatigue damage is equal to $1/(40*365*24*12)= 2.378*10^{-7}$. If the fatigue rate is larger than 1, then the ship will have a reduced lifetime if the current operating conditions were to continue, e.g. a rate of 10 indicates a lifetime for the vessel of $40/10= 4$ years if the present conditions were to continue for those 4 years. Hence if fatigue rate is 1 all time, a crack is expected on 2-3% of the details of the structure due to S-N curve used.

Similarly, the half hour fatigue rates can be calculated. Then, looking at maximum values, the 5 minutes fatigue rates are higher than 30 minutes fatigue rates where high loading events are less dominating.

However, it should be mentioned that fatigue damage is related to fatigue loading, while the real cracking may differ depending on different factors such as workmanship, SCF and coating conditions.

Results from Fatigue Analysis

The total 5 minutes fatigue rates and wave fatigue rates for the port and starboard sensors DMP and DMS in deck amidships are displayed in Figures 4.3 and 4.5. The vibration contribution to the total damage is 57.4% for DMP and 54.8% for DMS. The average total fatigue rates in air are 0.18 and 0.25 for the two sensors, respectively, which correspond to fatigue lives of 222 and 158 years. The maximum 5 minutes fatigue rates are 371.7 and 373 (the maximum half hour fatigue rates are 168 and 170 for the same sensors respectively). This shows more damage in starboard side then in port side by factor of about 1.4. Results from other sensors are displayed in Table 4.1.). In smaller container vessels (Storhaug G. , 2012).

The maximum half hour fatigue rates were 62 in 2800TEU and 98 in 4400TEU. These two vessel have 20 years target fatigue life, than fatigue rates are also high for the smaller vessels.

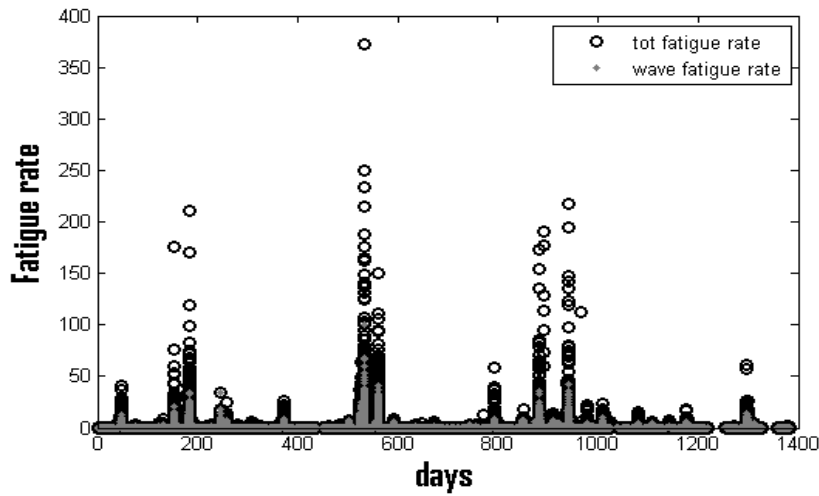


Figure 4.2: Total and wave 5 minutes fatigue rates for port side deck sensor (DMP)

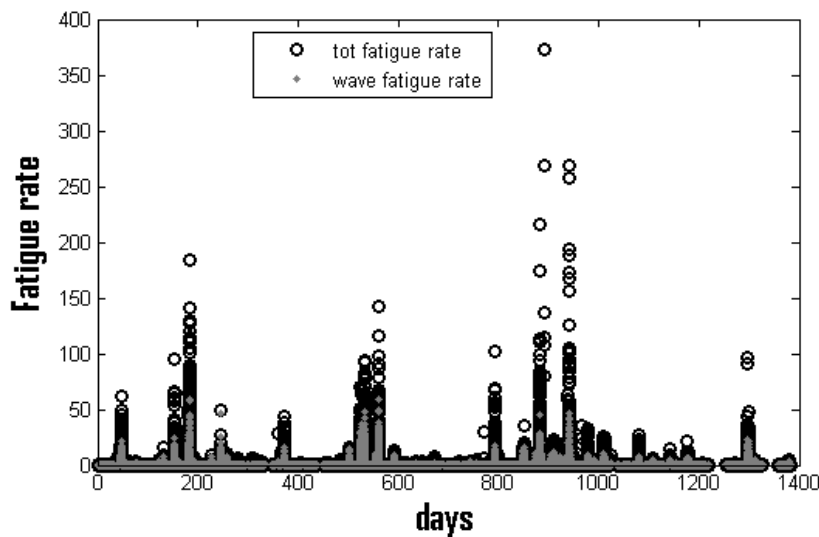


Figure 4.3: Total and wave 5 minutes fatigue rates for port side deck sensor (DMS)

Table 4.1:

Results from fatigue analysis for the different sensors.

Sensors	Max. fatigue rate	Max. wave fatigue rate	Mean fatigue rate	Fatigue life	Vibration contribution
DMS	373	59	0,253	158	54 %
DMP	371	99,95	0,18	223	57%

Chapter 4: Trade and Fatigue Loading Overview

ISS	42,9	15	0,04	1053	40 %
ISP	102	32	0,13	305	37 %
SWS	30	25	0,05	844	26 %
SWP	70	25	0,03	1424	33 %
SFS	36	6	0,02	2100	58 %
SFP	371	4	0,024	1680	69 %
DAS	152	24	0,06	661	65 %
DAP	362	26	0,1	394	62 %
IAS	46,5	4	0,005	9307	57,40 %
IAP	50	48,4	0,08	513	21 %
DFP	372	31,7	0,04	1041	60 %
DFS	57	12,4	0,02	2123	62 %

Fatigue analysis for welded details in corrosive environment

The Rainflow spectra from the different types of time series is saved at regular intervals of one hour and stored in Rainflow files e.g. RainfRaw, RaifDYN and RainfWAV. These stored Rainflow spectra enable reanalysis of the fatigue development of the vessel based on different parameters than pre-set in the configuration of the HMON system.

In the following, corrosive S-N curve (DNV2), (DNV, 2010) and SCF factor of 2 are used to recalculate the fatigue damage. For DMP and DMS the average fatigue rates are 0.55 and 0.81 respectively, which correspond to 72 and 49 years fatigue lives.

Fatigue damage for the different voyages

The plot of longitude from the measurements period in Figure 4.4 shows that the vessel has been trading between the same ports, and has performed 20 voyages, from North Europe to East Asia and back in a regular pattern. However the weather conditions vary from one voyage to the other. The Table 4.2 shows the performed voyages from the 3rd of June 2009 to the 18th of Mars 2013. The accumulated fatigue damage for each voyage for both deck sensors amidships DMP and DMS is illustrated in Figure 4.5. It seen that the accumulated fatigue damage is particularly large for voyage 17 and 27. This is because the worst 2 storms seen in Figure 4.3 have been encountered during these two voyages.

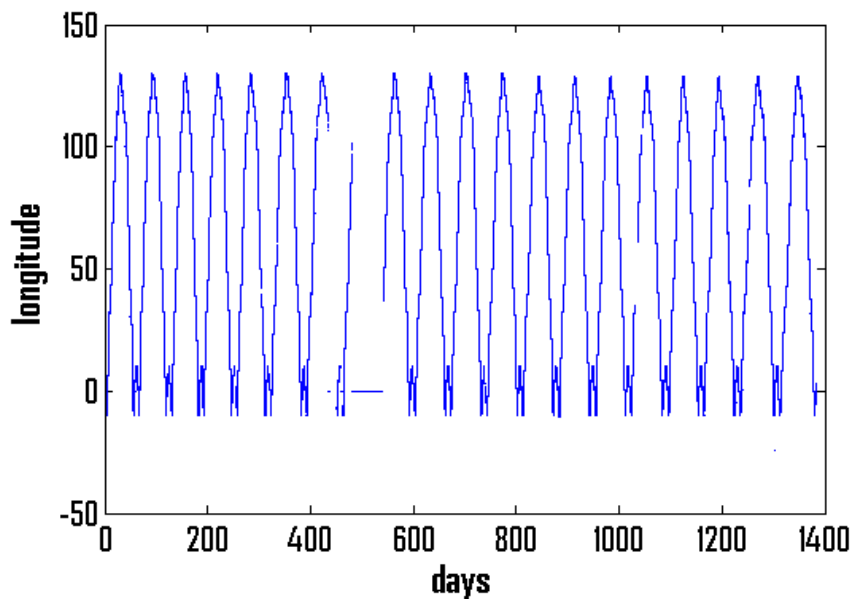


Figure 4.4: Longitude (negative is West, positive is East)

Table 4.2:

Voyages from the 3rd of June 2009 to the 18th of Mars 2013

Voyage	East		Voyage	West	
	From	To		From	To
1	2009-06-03	2009-07-03	2	2009-07-03	2009-08-04
3	2009-08-04	2009-09-04	4	2009-09-04	2009-10-06
5	2009-10-06	2009-11-06	6	2009-11-06	2009-12-07
7	2009-12-07	2010-01-07	8	2010-01-07	2010-02-10
9	2010-02-10	2010-03-12	10	2010-03-12	2010-04-16
11	2010-04-16	2010-05-21	12	2010-05-21	2010-06-25
13	2010-06-25	2010-07-30	14	2010-07-30	2010-09-03
15	2010-09-03	2010-10-08	16	2010-10-08	2010-11-12
17	2010-11-12	2010-12-18	18	2010-12-18	2011-01-21
19	2011-01-21	2011-02-25	20	2011-02-25	2011-04-01
21	2011-04-01	2011-05-06	22	2011-05-06	2011-06-10
23	2011-06-10	2011-07-16	24	2011-07-16	2011-08-19
25	2011-08-19	2011-09-25	26	2011-09-25	2011-10-27
27	2011-10-27	2011-12-04	28	2011-12-04	2012-01-09
29	2012-01-09	2012-02-11	30	2012-02-11	2012-03-16

31	2012-03-16	2012-04-22	32	2012-04-22	2012-05-28
33	2012-05-28	2012-07-01	34	2012-07-01	2012-08-05
35	2012-08-05	2012-09-09	36	2012-09-09	2012-10-14
37	2012-10-14	2012-11-24	38	2012-11-24	2012-12-31
39	2012-12-31	2013-02-08	40	2013-02-08	2013-03-18

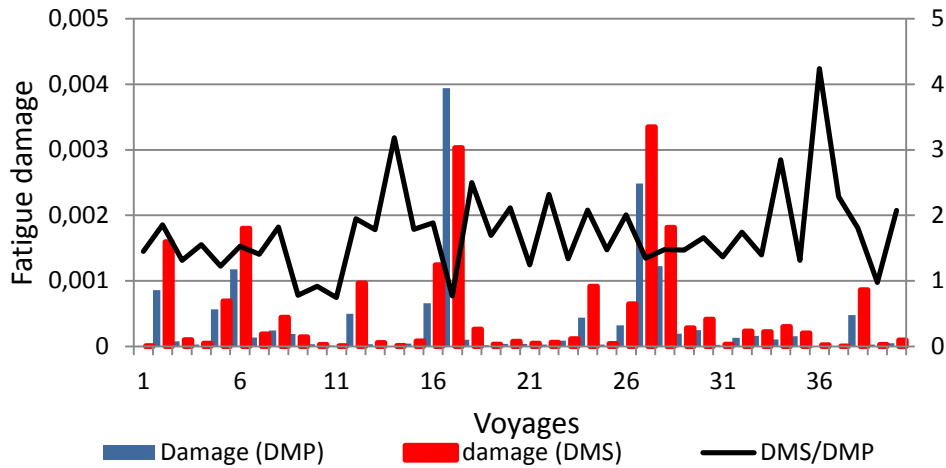


Figure 4.5: fatigue damage recorded each trip in the DMP and DMS sensors.

Dividing the damage from starboard sensor by the damage from the port sensor in Figure 4.5 show that most of the time (35 voyages) DMS had more damage than DMP sensors. In voyage 36, DMS has more than 4 times damage the DMP. This may be caused by the wind heading profile which could not be symmetric. This is investigated in the chapter 5.

Fatigue rate intervals

If we consider the port sensor in deck amidships (DMP), the time in different fatigue rate intervals and the contribution of the intervals to the total damage are displayed in Figure 4.6. The fatigue rate interval of 0.01-1 refers to the time spent between 0.01 and 1. Fatigue rates are summarized for each interval and divided by the total summarized fatigue rates. 83% of the time the fatigue rates are below 0.01 and the damage in this interval is only 0.4% of the total damage. 98% of the time the fatigue rates are below the design average of 1 and that corresponds to 11 % of the total damage. When we consider the interval of time where the fatigue rates are above 10, it consists of less than 0.5% of the total time while it accounts for 56% of the total damage. The higher fatigue rates are limited in time but critical regarding to damage contribution this may be reduced by routing or speed reduction in order to reduce

significantly the whipping contribution and damage in general. For this trade routing is not relevant, so only the speed reduction is considered effective. A few hours of speed reduction may significantly reduce the fatigue damage, and this vessel has plenty of power to catch up in calm seas. The average speed of the vessel at sea is 18 knots, which is quite low comparing to the available service speed (28 knots). It is noted that for the high fatigue rates (>50), the vibration contribution is higher than in the other fatigue rate intervals, 72%.

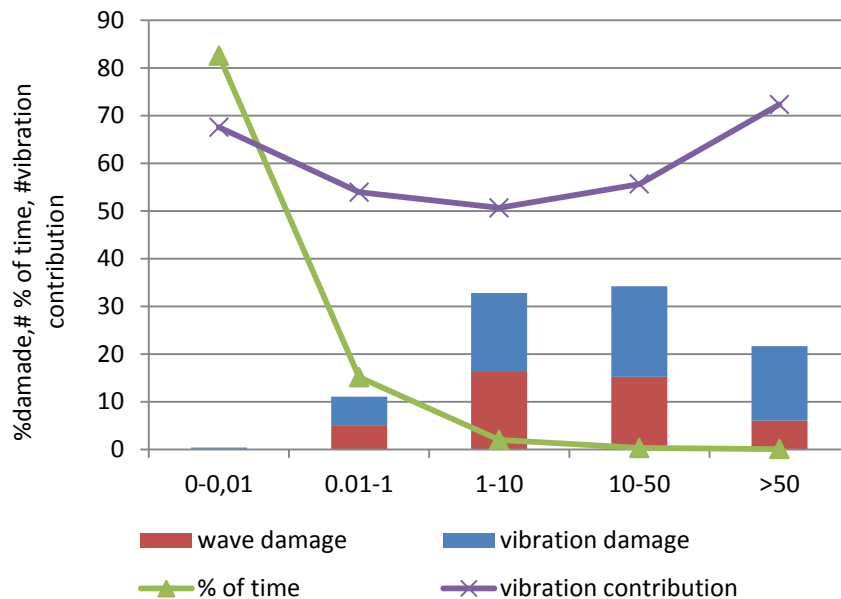


Figure 4.6: % of time and % of damage in the different fatigue rate intervals.

Conclusion

The fatigue is not regarded to be an issue if the vessel continues to operate in this East Asia to Europe trade. This may be due to the good vessel design based on CSA-2 class notation and 40 years target life, but it is also a consequence of the trade, which is expected less severe than World Wide trade, North Pacific or North Atlantic trade. This will be further examined in next chapter. However, some very some very high fatigue rates have been observed with high vibration contribution. The fatigue damage is not symmetric, the starboard sensor DMS show higher damage then the port sensor DMP. The storms with high fatigue rates are limited in time but very critical regarding contribution to the total damage, then proper seamanship are need to reduce these high fatigue rates.

Fatigue Damage versus Wind Conditions**Wind Profile**

The system receives also data from other ship systems, such as the GPS and the wind sensor. The collected wind data give the wind speed and direction relative to the ship every 5minutes. It should be noted that the wind sensor has not always been reliable during the period before 21st of December 2010, and due to these unreliable results the wind records before this date has been omitted in the following analysis. The remaining period covers 2.3 years of data. Before using the wind data in the analysis, it has to be corrected for the forward speed of the vessel as well as its relative heading. This is made by simple vector considerations which gave the following equations, 5.1 and 5.2

$$\beta_{real} = \tan^{-1} \frac{V_m * \sin(\beta_m)}{V_m * \cos(\beta_m) - V} \quad (5.1)$$

$$V_{real} = \frac{V_m * \sin(\beta_m)}{\sin(\beta_{real})} \quad (5.2)$$

Where, β_{real} is the corrected wind direction relative to the ship and V_{real} is the real wind speed. β_m and V_m are the measured wind direction and speed respectively, and V is the vessel speed.

The wind sensor is located about 43.5m above the sea surface. The wind speed has to be corrected down to 10m above the sea surface which is the reference for the Beaufort scale (DNV, .April, 2007.). This is shown in eq. 5.3

$$V_{10} = V_{real} * \left(\frac{10}{h}\right)^{1/7} \quad (5.3)$$

V_{10} is the wind speed at 10m above the sea surface while h is the sensor height in meter.

The wind speed is converted to Beaufort scale and the probability distribution of the wind as function of Beaufort number Bn is shown in Figure 5.1. Only measurements when the vessel speed was above 3 knots are considered. The records when the vessel is in “port area” are neglected in plotting the probability distribution. Comparing to Argoss data in open sea for the North Atlantic trade(excel sheet for DNV), the measured wind is much less severe. Bn number 3 is most frequent. Bn of 5 is most frequent from Argoss, which have much higher probabilities for higher Bn. This is as expected for this trade. East Asia to Europe is much less severe than North Atlantic.

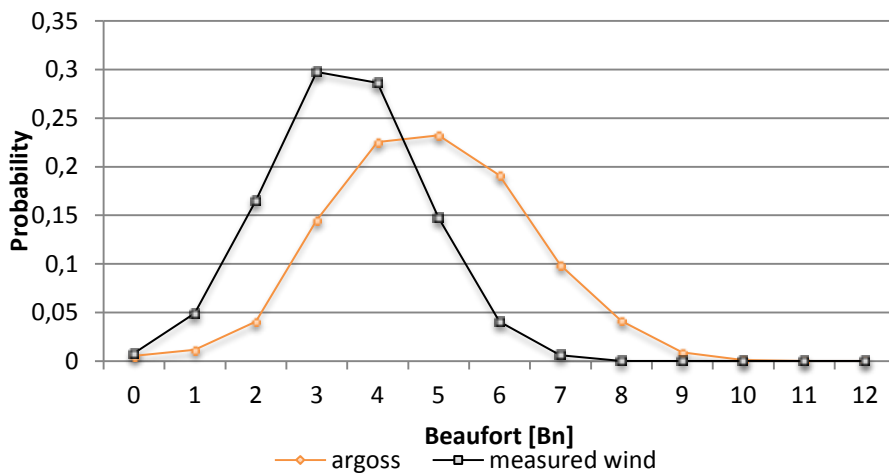


Figure 5.1: Measured wind strength distribution versus Argoss.

In table 5.1 Bn scale is converted to significant wave height H_s . Bn 3 which is most frequent, correspond to $H_s = 1$ m. For North Atlantic Bn 5 the most frequent correspond to $H_s = 2.5$ m. It clear that current trade is very “calm” comparing to the north Atlantic.

Table 5.1:

Beaufort scale versus significant wave height (Pear Drop)

Beaufort Scale and Probable Wave Height						
Beaufort number	Description term		Wind speeds		Wave height (m)	
	Wind	Wave	knots	m/s	probable	maximum
0	Calm	-	< 1	0 - 0.2	-	-
1	Light air	Ripples	1 - 3	0.3 - 1.5	0.1	0.1
2	Light breeze	Small wavelets	4 - 6	1.6 - 3.3	0.2	0.3
3	Gentle breeze	Large wavelets	7 - 10	3.4 - 5.4	0.6	1.0
4	Moderate breeze	Small waves	11 - 16	5.5 - 7.9	1.0	1.5
5	Fresh breeze	Moderate waves	17 - 21	8.0 - 10.7	2.0	2.5
6	Strong breeze	Large waves	22 - 27	10.8 - 13.8	3.0	4.0
7	Near gale	Large waves	28 - 33	13.9 - 17.1	4.0	5.5
8	Gale	Moderately high waves	34 - 40	17.2 - 20.7	6.0	7.5
9	Strong gale	High waves	41 - 47	20.8 - 24.4	7.0	10.0
10	Storm	Very high waves	48 - 55	24.5 - 28.4	9.0	12.5
11	Violent storm	Exceptionally high waves	56 - 63	28.5 - 32.6	11.5	16.0
12	Hurricane	Exceptionally high waves	64 - 71	32.7 - 36.9	14.0	> 16
13	Hurricane	Exceptionally high waves	72 - 80	37.0 - 41.4	> 14	> 16
14	Hurricane	Exceptionally high waves	81 - 89	41.5 - 46.1	> 14	> 16
15	Hurricane	Exceptionally high waves	90 - 99	46.2 - 50.9	> 14	> 16
16	Hurricane	Exceptionally high waves	100 - 109	51.0 - 56.0	> 14	> 16
17	Hurricane	Exceptionally high waves	109 - 118	56.1 - 61.2	> 14	> 16

The average five minutes fatigue rates and the vibration contribution to fatigue damage as function of Beaufort strength are displayed in Figure 5.2. The vibration contribution increase with the increase of the wind strength, from 34% for Bn=1 to 73% for Bn=9. The average five minutes fatigue damage increase with the wind and it exceeds the budget fatigue damage for Bn=7 and above. It should be noted that the average fatigue rates are low as a result of all headings being included. This also affects the vibration contribution, which is expected low in

e.g. beam seas and wind conditions. The total average fatigue rates increases faster than the vibration contribution

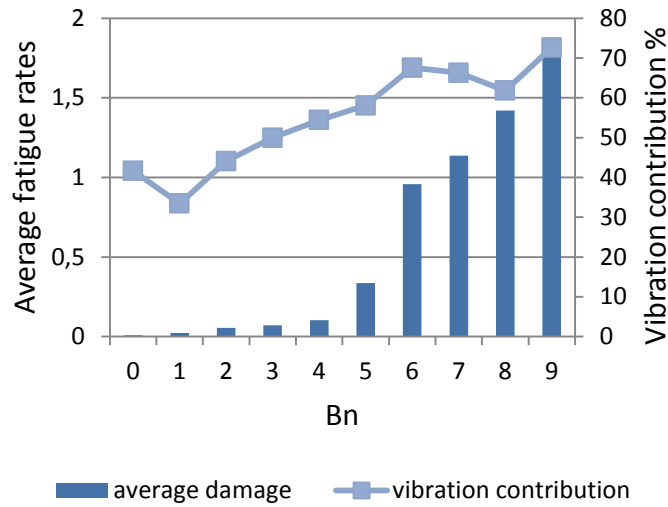


Figure 5.2: Average 5 minutes fatigue rates and vibration contribution as function of Bn.

The relative wind direction can be divided into 6 sectors. Head wind is defined as $0 \pm 30^\circ$, which refer to sector 1, while stern wind is $180 \pm 30^\circ$, which refers to sector 6. The other sectors have 30° steps and port and starboard observations are merged, see Figure 5.3.

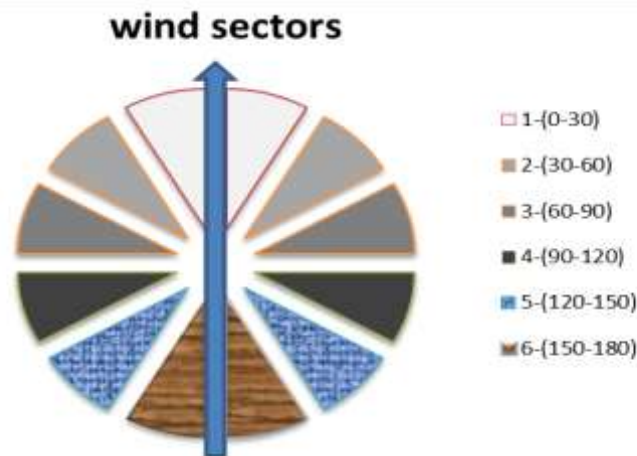


Figure 5.3: Wind sectors.

The relative wind heading distribution is displayed in Figure 5.4, which shows that the stern and head winds are dominating with 31% and 24 % encounter probability, respectively. The average probability is $100/6 = 16.7$. Stern wind counts about 2 times the average encountered probability. The true wind is the relative the north. It may be estimated by summarizing the

course over ground of the vessel δ with the corrected wind direction β_{real} , eq. 5.4. Further, the obtained values which are over 360° have to be corrected subtracting 360. Or by:

$\beta_{true} = remainder(\beta_{true}, 360)$ if we have a vector of value

$$\beta_{true} = \beta_{real} + \delta \tag{5.4}$$

The true wind distribution, illustrated in the Figure 5.5, show that the wind is quite evenly distributed between the 6 sectors. Northern (wind coming from northern) and northeastern winds are, however, slightly prevailing. This is expected for the Northern Indian Ocean where the ship spends a relatively high part of the time.

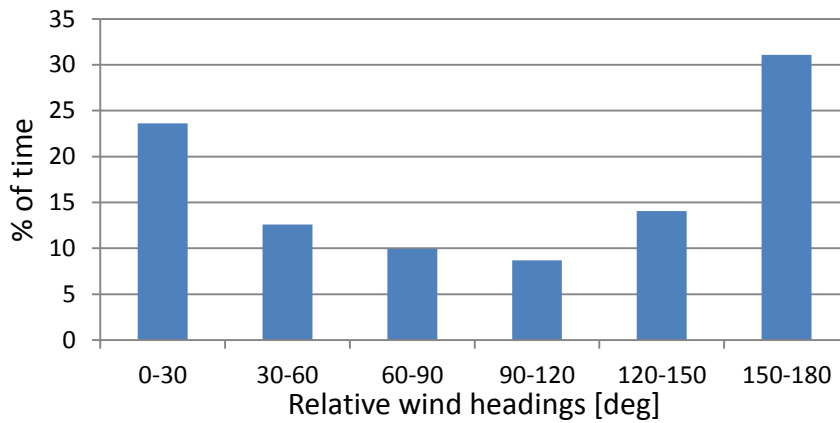


Figure 5.4: Relative wind heading profile.

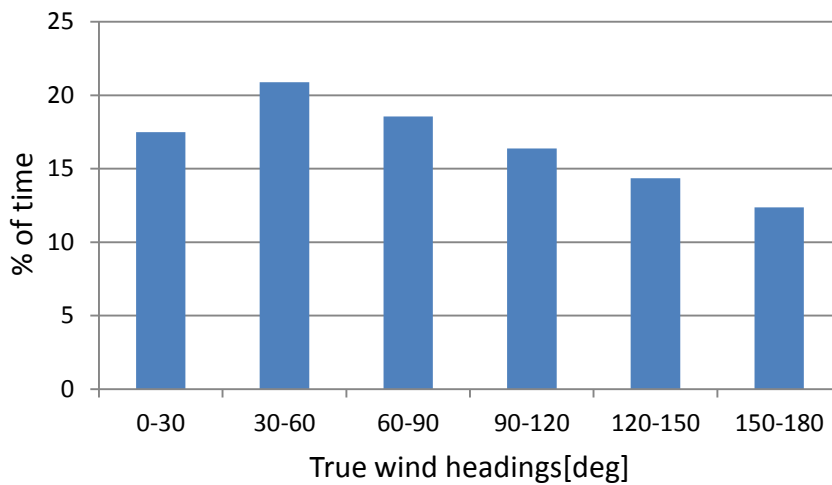


Figure 5.5: True wind heading profile

Fatigue Damage versus Wind Headings

Figures 5.6~5.7 show the percent of damage and vibration damage contribution as function of wind headings, for both sensors DMP and DMS. Head and bow quartering winds are much more important than other headings with 29.5% and 28.3% contribution, respectively, for the DMP sensor. While beam winds (sector4) have the lowest importance with 4.4% for the DMP sensor. It is clear that the vibration contribution decays from bow quartering, 66%, to stern seas, 44%. The DMP and DMS shows consistent results, but the differences can be explained by the heading profile not being completely symmetric, this is studied later on in this chapter. Another significant observation is that vibration is clearly present also in stern winds, which also have been observed on other container vessels (Storhaug, G, 2012).

Tables 5.2~5.3 show the fatigue damage versus wind headings. Based on the average fatigue rates and the probability for each heading, the wind headings are rated from the most critical regarding to fatigue damage to the least critical. Results are identical for both sensors DMP and DMS, and sectors 2 and 3 are considered the worst headings. The reason for head wind not producing worse results could be because the encountered sea states can be considered relatively small for this long vessel (340m LOA), so it is quartering seas that gives more significant wave bending moment as the wave length then appears longer. This will similarly affect stern wind heading. Further, in stern seas also the frequency of encounter is reduced compared to head seas, which results in fewer fatigue cycles per hour and thereby also lower fatigue damage in general.

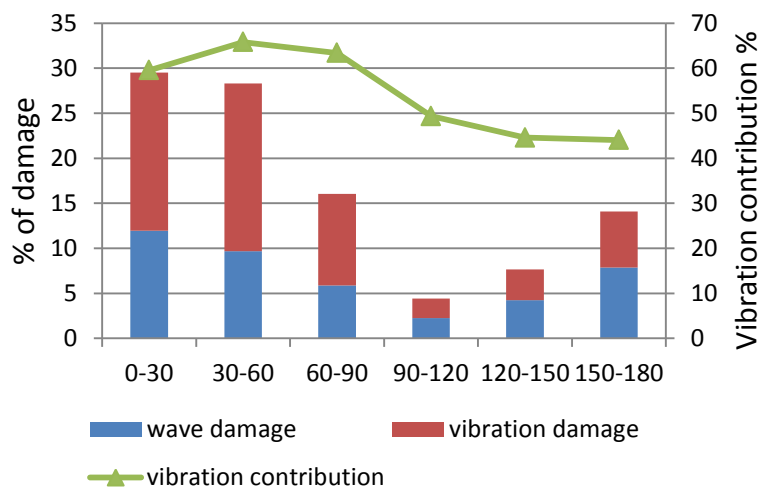


Figure 5.6: % of damage and relative wave/vibration damage versus wind sectors (DMP)

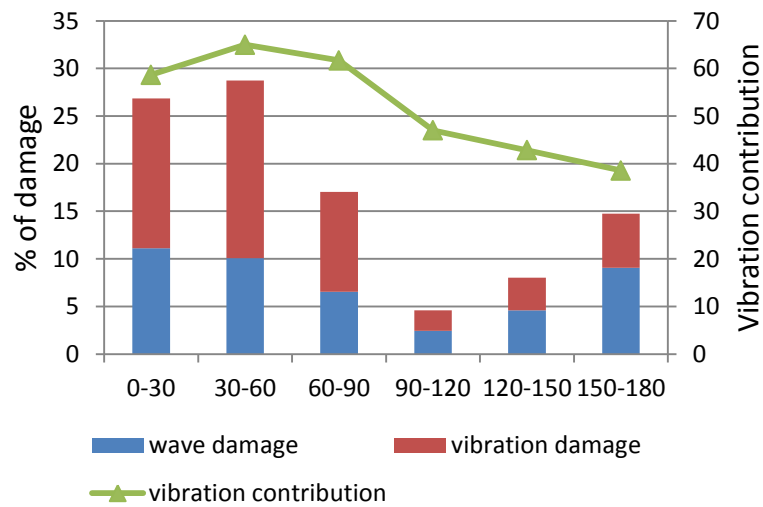


Figure 5.7: % of damage and relative wave/vibration damage versus wind sectors (DMS).

Table 5.2:

Fatigue damage versus wind heading (DMP)

Wind sectors	%time	Damage/sector	Av. damage	Rating
0-30	23,6	29,5	0,17	3
30-60	12,6	28,3	0,31	1
60-90	10,0	16,1	0,22	2
90-120	8,7	4,43	0,07	5
120-150	14,1	7,64	0,07	4
150-180	31,1	14,1	0,06	6

Table 5.3:

Fatigue damage versus wind heading (DMS)

Heading	%time	% Damage/sector	Av. damage	Rating
0-30	23,6	26,85	0,24	3
30-60	12,6	28,72	0,49	1
60-90	10,0	17,05	0,38	2
90-120	8,7	4,59	0,11	5
120-150	14,1	8,03	0,12	4
150-180	31,1	14,76	0,10	6

Sector 2

Considering the sector 2, which is the most critical wind heading, Figures 5.8~5.9 show the corresponding total damage distribution, relative vibration contribution, average five minutes damage and average speed for each Bn number. It should be noted that Bn 0 and Bn 7 have few observations. The average damage increases with increasing Bn, and it exceeds significantly the design budget damage for Bn 6 and 7. The vibration contribution increases from 30% for Bn 1 to about 73% for Bn 7. Bn=6 is the most contributing to fatigue damage with about 38%. The maximum average speed is about 17 knots and decrease slightly after Bn 2.

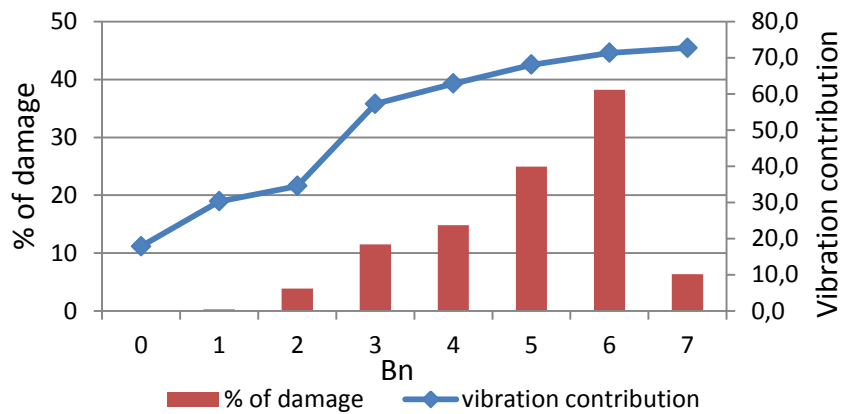


Figure 5.8: % of damage and vibration contribution versus Bn in sector2 (DMP)

Bn	0	1	2	3	4	5	6	7	8	9
Obs.	13	1024	4092	5036	3937	1912	840	104	0	0

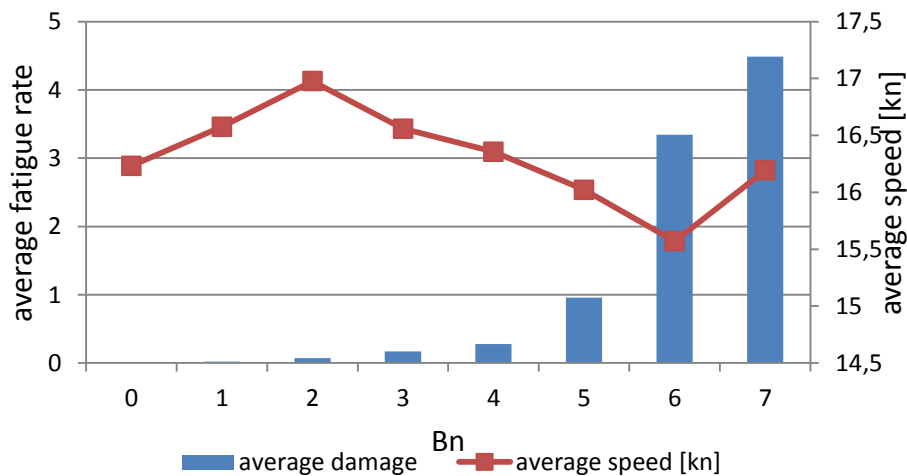


Figure 5.9: Average fatigue rates and average speed versus Bn in sector 2 (DMP).

Sector 1

The head wind (sector1) contributes most to fatigue damage for DMP sensor. The same diagrams are shown in Figures 5.10~5.11. There are few observations for high Bn 8 and 9 as well as Bn 0. The average damage has tendency to increase with increasing Bn to about 1.3 for Bn 7, while it decays again for Bn 8 and 9 (only 3 observation for Bn 9). It may happen that Bn 9 is related to the vessel being close to shore and that the waves actually are small due to short fetch even though the wind is strong. The vessel speed decreases with increasing Bn, and significant speed reduction is observed at Bn 8 and 9. This may also affect the vibration contribution and average fatigue damage. Bn 6 contributes most to fatigue damage with 36%. The vibration contribution to fatigue damage increases with Bn from 32% for Bn 1 to 79% for Bn 9. The results for sector 1 are in fair agreement with sector 2.

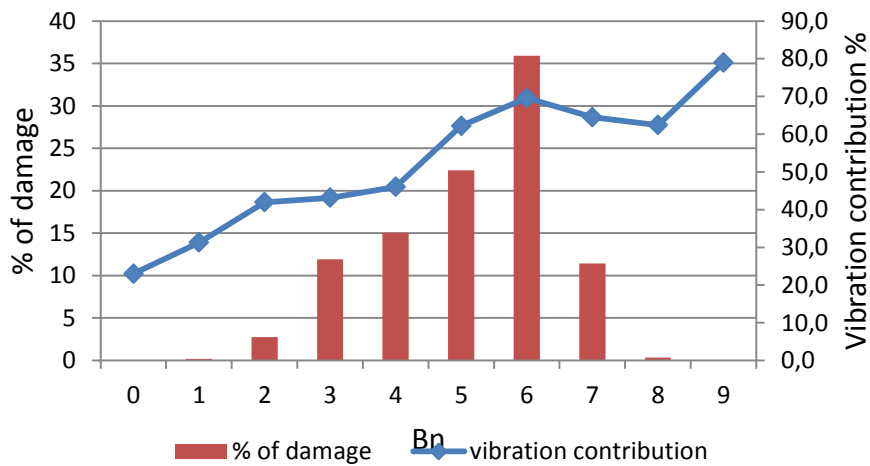


Figure 5.10: % of damage and vibration contribution versus Bn in sector1 (DMP)

Bn	0	1	2	3	4	5	6	7	8	9
Obs.	33	1184	4413	8423	10961	6809	2631	731	40	3

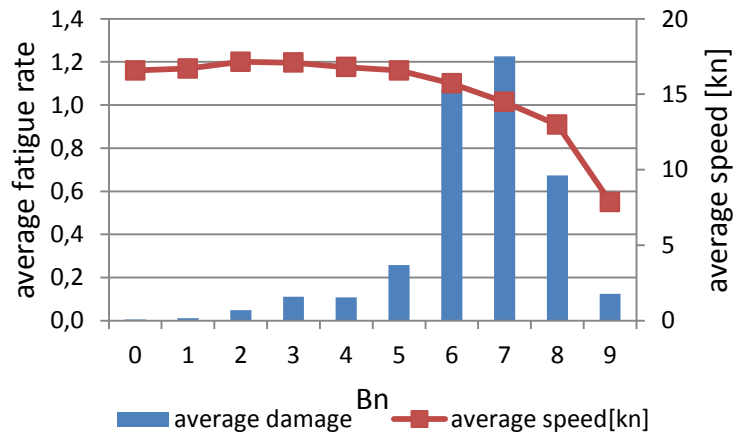


Figure 5.11: Average fatigue rates and average speed versus Bn in sector 1 (DMP).

Sector 3

For sector 3, the total damage and vibration contribution versus Bn are displayed in Figure 5.12 and the average 5 minutes fatigue rates with the average speed as function of Bn are displayed in Figure 5.13. There are few observations for high Bn 0 and 7. Bn 5 contributes most to the fatigue damage, about 50%. The vibration contribution increases with increasing Bn, from 32% for Bn 0 to 75% for Bn 7. The average damage is very low until Bn 4, and then it becomes significant for Bn 5, 6 and 7. It is over 5 times the budget damage for Bn 7 which has very few observations. The average speed increases from 16.5 knots at Bn 0 to 19 knots for Bn 7.

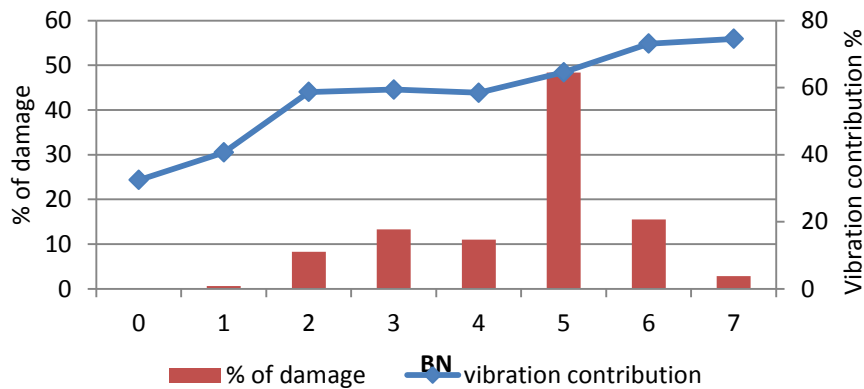


Figure 5.12: % of damage and vibration contribution versus Bn in sector 3 (DMP)

Bn	0	1	2	3	4	5	6	7	8	9
Obs.	42	1301	3873	4182	3096	1326	390	23	0	0

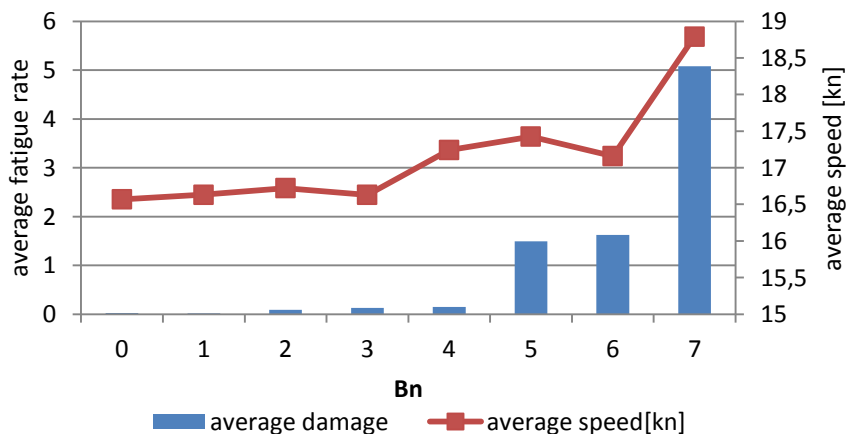


Figure 5.13: Average fatigue rates and average speed versus Bn in sector3 (DMP).

Sector 6

For stern seas (sector 6), the total damage and vibration contribution versus Bn are displayed in Figure 5.14 and the average 5 minutes fatigue rates with the average speed as function of Bn are displayed in Figure 5.15. The average damage is quite low even for Bn up to 7, while significant for Bn 8 and 9, which has few observations. , The vibration contribution does not show a clear trend and varies between 26% for Bn 5 to 70% for Bn 9. The average speed increases with increasing Bn as expected and observed on other container ships (Storhaug 2012). Bn 4 contributes most to the fatigue damage for stern seas in sector 6. The results are quite different from sector 1 and 2, but vibration effects are still present and significant in stern wind.

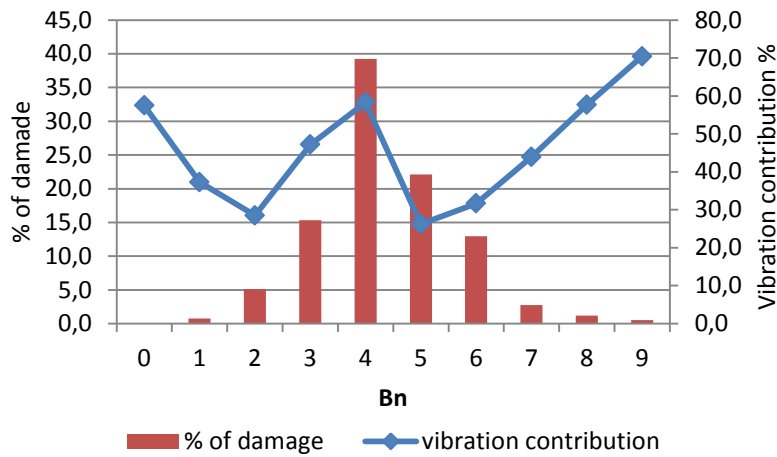


Figure 5.14: % of damage and vibration contribution versus Bn in sector 6 (DMP)

Bn	0	1	2	3	4	5	6	7	8	9
Obs.	356	1449	6345	15247	20614	9377	3056	557	51	9

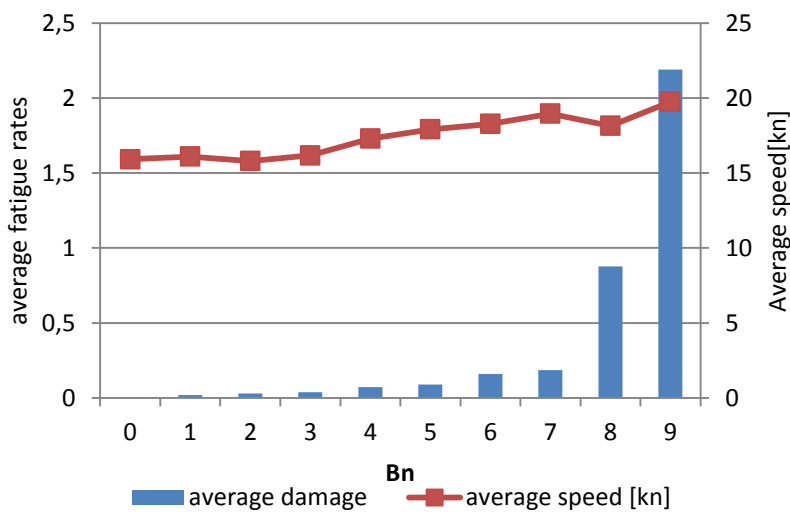


Figure 5.15: Average fatigue rates and average speed versus Bn in sector6 (DMP).

Sector 5

For sector 5, the same diagrams are shown in Figure 5.16 and 5.17 as for the other sectors. There are few observations for high Bn 7, 8 and 9. The vibration contribution tend to increase with increasing Bn, from 46 % for Bn 2 it decays down to 39 % for Bn 4 and increase again to 80% for Bn 9. The averages speed is between 16 and 17 knots and it decrease slightly for Bn 9. As in sector 3, Bn 5 contributes most to the fatigue damage in sector 5, and the average damage is very low for Bn below 4 and increase considerably to become very significant for Bn 8, over 6 times the budget damage. The average damage decreases again for Bn 9 to 2.5 the budget damage. This may be due the speed reduction.

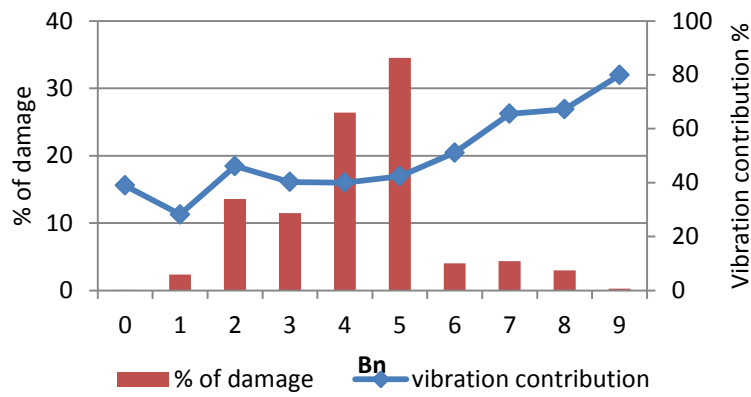


Figure 5.16: % of damage and vibration contribution versus Bn in sector 5 (DMP)

Bn	0	1	2	3	4	5	6	7	8	9
Obs.	35	1315	5686	8059	7113	2158	278	58	9	2

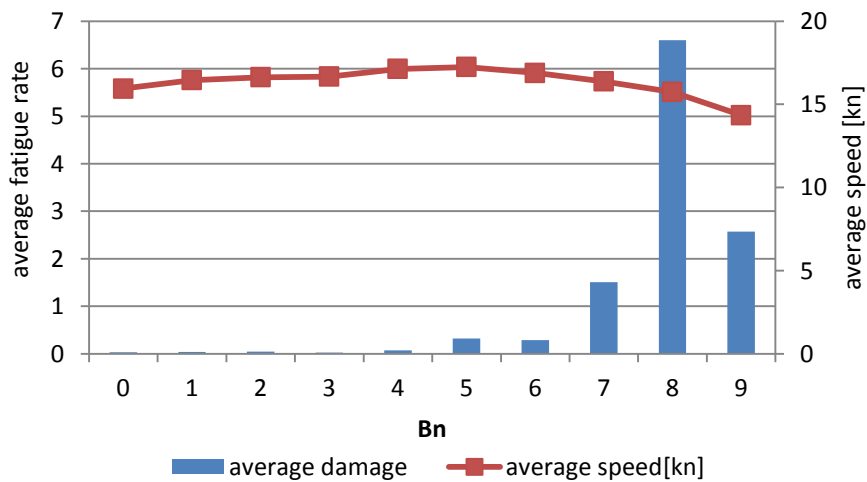


Figure 5.17: Average fatigue rates and average speed versus Bn in sector5 (DMP).

Sector 4

The wind from sector 4 was between Bn 1 and Bn 4 most of the time, 97%. There are very few observation for Bn 6, 7 and 8 as well as Bn 0. This may be the reason that this sector has the lowest average damage, 0.07, and contributes by only 4.4 % to the total damage (see Table 5.1).

Figure 5.18 shows the total damage and vibration contribution as function of Bn in sector 4, while average damage and average speed versus Bn are illustrated in Figure 5.19. Similar to sectors 3 and 5, Bn 5 contributes most to the fatigue damage, and the average damage is very low for Bn below 4 and increase significantly to exceed 12 times the budget damage for Bn 8, (only 1 observation). The vessel speed is reduced to 13 knots for Bn 7, and this led to reduction of the average damage. The vibration contribution tend to increase with increasing Bn.

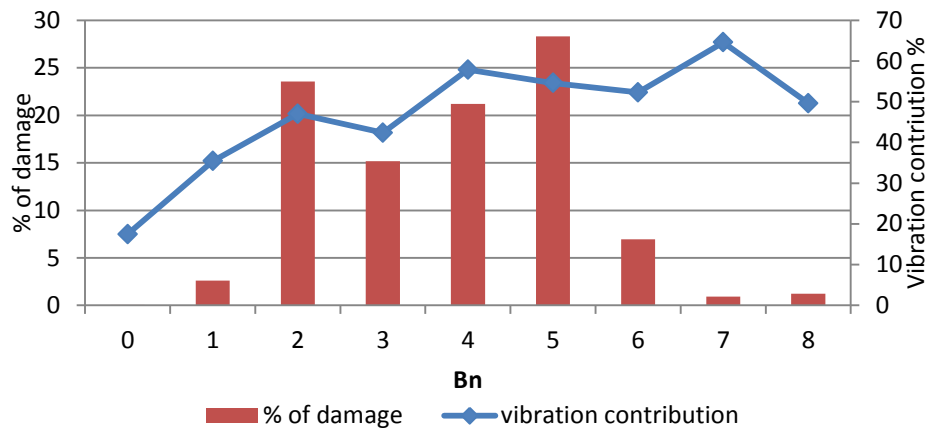


Figure 5.18: % of damage and vibration contribution versus Bn in sector 4 (DMP)

Bn	0	1	2	3	4	5	6	7	8	9
Obs.	39	1245	4047	4905	2487	385	19	5	1	0

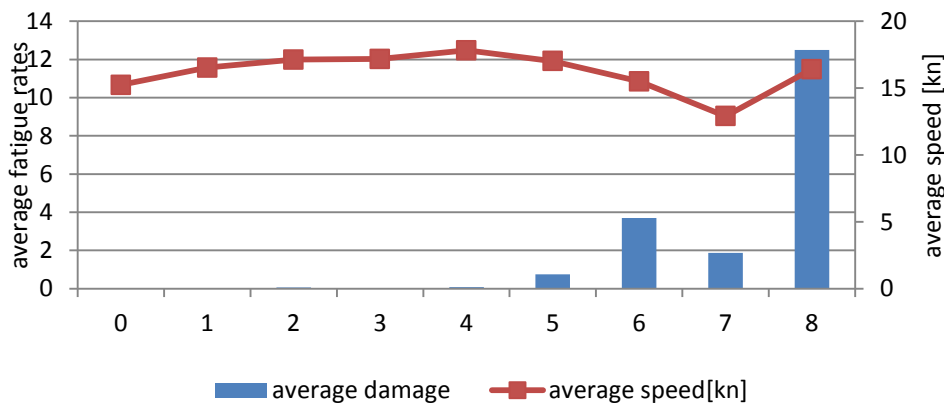


Figure 5.19: Average fatigue rates and average speed versus Bn in sector4 (DMP).

Wind profile for both port and starboard side

Figure 5.20 show the separated wind headings for port and starboard sides. In general, results are quite symmetric for both sides, with the stern wind to be higher in port side. Table 5.3 show the summarized 5 minutes fatigue rates in the different headings for both sensors, and the ratio of these values define the difference in damage between the 2 sides. This difference is significant in all in all the wind headings. Totally DMS have 57% higher damage then DMP (only the period after the 21st of December 2010 is considered here). It is clear that the heading profile is not the reason for the difference in damage between starboard and port deck sensors (DMS and DMP). Therefor it is not easy to explain this difference with the available data. It may be result of the setup of the sensors during the installation. During the installation the sensors should have been calibrated against the still water bending moments at 0 degree of vessel's heel. If the heel was higher than 0 during the calibration, that would contribute to the difference of stress results from the 2 sensors. Also wave heading profile could be a reason for this difference if it is not symmetric.

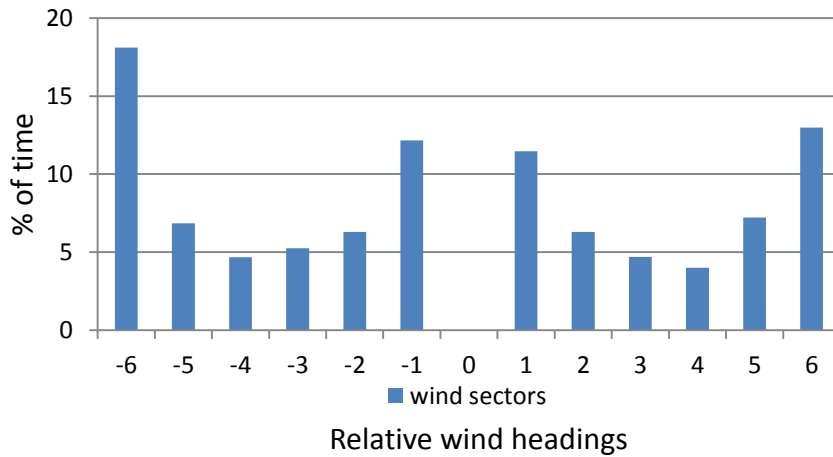


Figure 5.20: Relative wind headings for port (negative) and starboard (positive).

Table 5. 4:

Summarized 5 minutes fatigues rates in different wind headings for both sensors DMP and DMS.

Headings	1	2	3	4	5	6	Total
DMP	7983	7661	4338	1199	2068	3812	27062
DMS	11443	12239	7265	1955	3423	6290	42625
Ratio	1.4	1.6	1.67	1.63	1..65	1.64	1.57

The effects of voluntary speed reduction

A voluntary speed reduction in harsh environment may be effective to reduce the fatigue damage and in particular the vibration contribution in head and bow quartering seas. In Fig. 19, the fatigue rates for starboard deck sensor DMS are shown together with ship speed, wind relative heading and Beaufort strength for the day 30th December 2011. A relative scale is used for better comparison. The vessel was sailing in the Strait of Sicily, north of Tunisia (one of the severest areas in the Mediterranean Sea in December). The period with high fatigue rates lasts for about ½ a day. The average 5 minutes fatigue rate during this day is 29, meaning that 29 days of budget is spent. The speed is reduced from about 21 to 13 knots. Hence, the fatigue rates were reduced significantly. If the speed were reduced 9 hours earlier, the average fatigue rates would have been reduced further during this day and possibly the fatigue damage from this day could have been reduced down to 1/3. For this vessel it is not critical, but encountering such storms frequently, e.g. once on each crossing in a North Atlantic trade would result in undesirable low fatigue life.

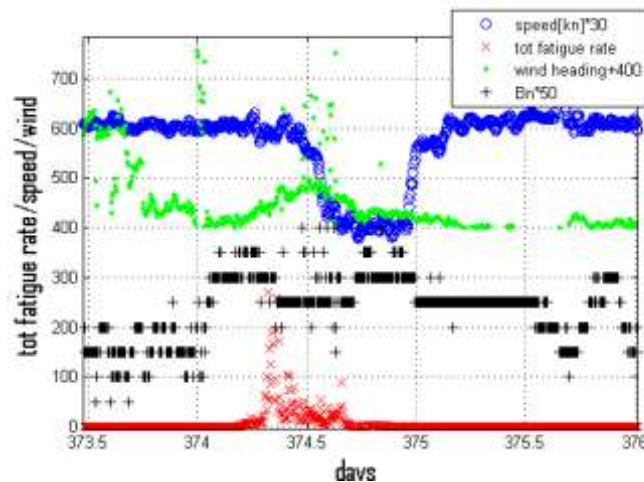


Figure 5. 21: Fatigue rates (DMS), vessel speed, wind heading, Bn, 30th December 2011.

Chapter 6**Fatigue Spectral Analysis****General**

There is fairly general consensus that the Rainflow counting technique provides the most accurate estimate for the fatigue damage of stochastic signals. However, in order to reduce the statistical uncertainty and obtain stable fatigue damage estimates, a large number of time series with durations long enough have to be provided and this requires relatively time-consuming analysis, (Nilsen, 2011)

In hull monitoring system the rainflow data is saved continuously and this requires significant storage capacity. Therefore, spectral analysis may be in some cases preferred for fatigue damage estimation, especially when the fatigue prediction is needed at locations where there are no measurements.

In ideal narrow-band process, where the power spectral density function has only one peak the fatigue damage is often estimated by narrow band approximation. In marine technology and offshore engineering, linear structural responses due to waves can usually be assumed to be Gaussian and narrow-banded with a spectral peak commonly corresponding to the peak frequency of wave input (Gao 2007). Moreover, many other responses might show bimodal spectral properties, e.g. the linear wave induced combined with springing/whipping responses. Many frequency-domain methods have been proposed for estimating wide-band Gaussian fatigue damage on the basis of spectral analysis, when the damage is estimated by a narrowband approximation and multiplied by a bandwidth correction factor.

For multimodal process the power spectral density function has multiple peaks at certain well separated modes, see figure 6.1 which illustrate the power density function of the stress measured in the DMP sensor, 17th November 2010. It is clear that the stress response is a bimodal process (two peaks at the stress spectrum). The wave linear response which is shown for ω between 0 and 1.5 rad/s and the high frequency response which is between 2.5 and 3.5 rad/s.

For bimodal process, specific methods have been proposed by several researchers such as (Jiao et al 1990) and (Sakai 1995). In this case the fatigue damage is estimated by combination of the two frequency components. The method presented in (Jiao 1990)

accurately predicts the bimodal fatigue damage and has been widely used in many offshore codes, such as (DNV-OS, 2004) And it was also investigated in (Gao et al 2007) and generalized for estimating trimodal fatigue damage. In this chapter, the fatigue damage is estimated based on the Jiao and Moan method. And results are compared to Rainflow counting's results.

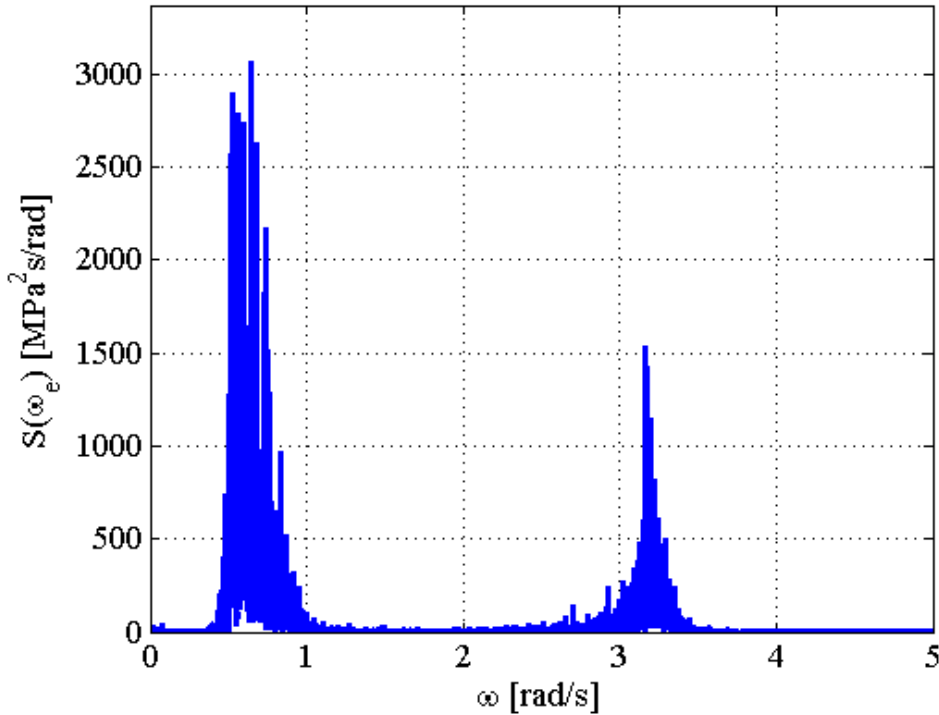


Figure 6.1: The stress spectrum measured for DMP, 17th November 2010 -22:00

Jiao and Moan Method

For a narrow banded Gaussian stress process, the stress amplitude follows a Rayleigh distribution eq. 6.1 (Jiao 1990):

$$f_R(r) = \frac{r}{\sigma_x^2} \exp\left(-\frac{r^2}{2\sigma_x^2}\right)$$

(6.1)

In this case the expected damage, D_{NB} over a period T is estimated by the following formula:

$$D_{NB} = \frac{\nu_0 T}{\bar{a}} (2\sqrt{2}\sigma)^m \Gamma\left(\frac{m}{2} + 1\right) \quad (6.2)$$

Here m and \bar{a} are the slope and the scale factor respectively, in the S-N curve. ν_0 is the mean zero-up-crossing frequency, while σ is the standard deviation of the stress signal. R is the stress amplitude and Γ is gamma function.

By applying the narrow band approximation (eq. 6.1) to the wide banded stress the Rayleigh stress range distribution will assign higher probabilities to the larger stress cycles. In this case the estimation fatigue damage is conservative.

Therefore, by applying the procedures of Jiao and Moan, the stress response is divided into two components, a stationary narrow-banded LF process and transient process HF. The stationary part here is taken as the wave frequency response, while the transient part as the vibration response. This method is based on the following assumptions:

- The initial amplitude of the arrival transient component is a random variable and follows a Rayleigh distribution; this is in agreement with theoretical findings in (Jensen et al 2009).
- The stationary narrow-banded and the transient are assumed to be independent. In reality, the whipping event is not separated in time with a wave induced sagging peak (Ulrik 2011) and that may lead to slightly conservative results.
- Any possible high frequency steady state (springing) is included in the transient process. As the whipping and springing cannot be separated in the measured stress signal that could be acceptable even though is not purely in accordance with Jiao and Moan method.

The fatigue damage expected over a time period T is estimated, according to Jiao and Moan, from the tow individual components. The first components is $P(t)$ which is the envelope of the total stress process and it is approximated as the sum of the low frequency part $X_1(t)$ and the Cramer and Leader C-L envelope $R_2(t)$ of the transient process $X_2(t)$ (Van dyck 1981):

$$P(t) = X_1(T) + R_2(t) \quad (6.3)$$

$$D = D_p + D_2 \quad (6.4)$$

$$D_p = \frac{\nu_{0,1} T}{\bar{a}} (2\sqrt{2\sigma_1})^m \Gamma\left(\frac{m}{2} + 1\right) \eta(T_0) \quad (6.5)$$

$$D_2 = \frac{T}{T_0 \bar{a}} (2\sqrt{2\sigma_2})^m \Gamma\left(\frac{m}{2} + 1\right) \frac{1}{1 - \exp(-2\pi\xi m)} \quad (6.6)$$

Where D is the total damage, D_p represent the damage due to the envelope $P(t)$ and D_2 is the damage from the transient process. σ_1 and σ_2 are the standard deviation of the low frequency part $X_1(t)$ and the transient part $X_2(t)$ respectively. $\nu_{0,1}$ is the mean zero up-crossing rate of $X_1(t)$. T_0 is a constant mean period of the arrival time between each whipping event. ξ is the total damping ratio. Γ is the gamma function, \bar{a} and m are the scale factor and the slope of the S-N curve. And the correction factor $\eta(T_0)$ is defined in eq. 6.7:

$$\begin{aligned} \eta(T_0) = & \frac{1}{T_0} \int_0^{T_0} \frac{1 - \theta \exp(-\xi\omega_2 t)}{[1 + \theta^2 \exp(-2\xi\omega_2 t)]^3} dt \\ & + \frac{\sqrt{\pi} m \theta \Gamma\left(\frac{m}{2} + \frac{1}{2}\right)}{T_0 \Gamma\left(\frac{m}{2} + 1\right)} \int_0^{T_0} \exp(-\xi\omega_2 t) [1 + \theta^2 \exp(-2\xi\omega_2 t)]^{\frac{m}{2}-2} dt \end{aligned} \quad (6.7)$$

Where $\theta = \frac{\sigma_2}{\sigma_1}$ and $\omega_2 = 2\pi * \nu_{0,2}$ and $\nu_{0,2}$ is the mean up-crossing ratio of the transient process $X_2(t)$.

Assuming $u = \theta \exp(-\xi\omega_2 t)$

$$du = -\theta \xi \omega_2 \exp(-\xi\omega_2 t) dt = -\xi \omega_2 u dt$$

Hence, the integrals in eq.6.7 can be evaluated when $m = 3$ using the following formulas (Ulrik 2011):

$$\int \frac{u}{u(1+u^2)^3} du = \frac{1-u}{4(1+u^2)^2} + \frac{4-3u}{8(1+u^2)} + \ln\left(\frac{u}{\sqrt{1+u^2}}\right) - \frac{3}{8} \tan^{-1} u$$

$$\int \frac{du}{\sqrt{1+u^2}} = \ln(u + \sqrt{1+u^2})$$

Application of Jiao and Moan spectral method

In the following, the fatigue damage is estimated from times series measured in amidships deck sensor DMP based on both spectral method (Jiao and Moan) and time domain (Rainflow counting). Based on the Rainflow files the fatigue damage is estimated in hourly basis using one slope S-N curve, with $m = 3$ and $\log(\bar{a}) = 12.65$, and stress concentration factor of 2. For the spectral method the same parameters have been used. And finally the accumulated damage during an observation interval of one hour is scaled by the target lifetime of the vessel to obtain hourly fatigue rates. Two cases have been assessed. The first, the stress was measured at moderate environmental condition, and the second is taken from the worst encountered storm.

Case one:

The stress time series from the 1st of December 2011 – 00:00 to the 2nd of December 2011 – 23:59 have been used. The vessel was sailing in East China sea, see figure 6.2. The wind strength was between 3 and 5 Beaufort, and 75% of the considered period the vessel encountered head and bow quartering headings. The average speed was 16 knots. The mean period of the arrival time between each whipping event is estimated graphically from the stress time series as $T_0 = 60s$. The damping ratio of the vessel is taken as 0.02. Results of the estimated fatigue rates from narrow banded approximation (Dnb), Jiao and Moan method (D), and Rainflow counting (RFT) are illustrated in figure 6.3. Most of the time D is slightly higher than RFT, only for 05:00, 08:00 and 12:00 RFT exceeds slightly D. The summarized fatigue rates during these two days gives 102 for D and 93 for RFT. As it is expected, the narrow band-approximation is higher than D and RFT, and it constitutes an upper bound to the rainflow counting results, in agreement with the findings in (Rychlik, 1993) The estimated damage from Jiao and Moan method is in good agreement with the Rainflow damage.

In figure 6.4, the estimated spectral hourly fatigue rates from the wave responses is presented and high frequency contribution to the total damage as is estimated with both methods, spectral and rainflow counting, is illustrated. The high frequency curves have the same general trend; they low when the total stresses are high. The minimum high frequency contribution is recorded the first day at 19:00, 19% is estimated by the spectral method and 36 % by the rainflow counting. For day 2, the low stresses have been recorded and high frequency curves increases significantly to reach 82 % for the spectral method and 97 % for

the rainflow counting. The vibration contribution curve of the rainflow counting is always above the curve of the spectral method. For the rainflow counting all the small stress cycles are counted, while for the spectral method the larger probabilities are given the large stress cycles, (Jiao and Moan). This may be the reason why the estimation of vibration contribution is higher when is estimated by the Rainflow counting method.

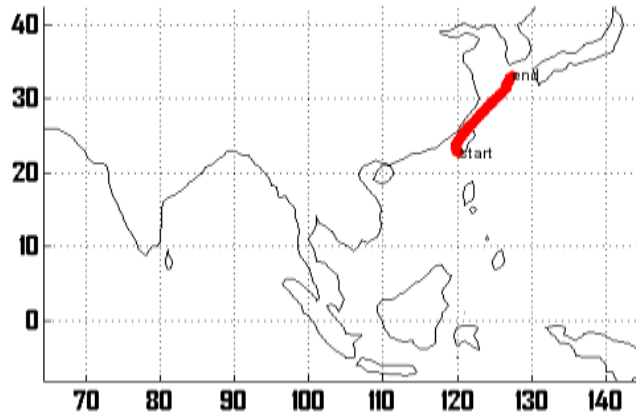


Figure 6.2: The position of the vessel in case 2.

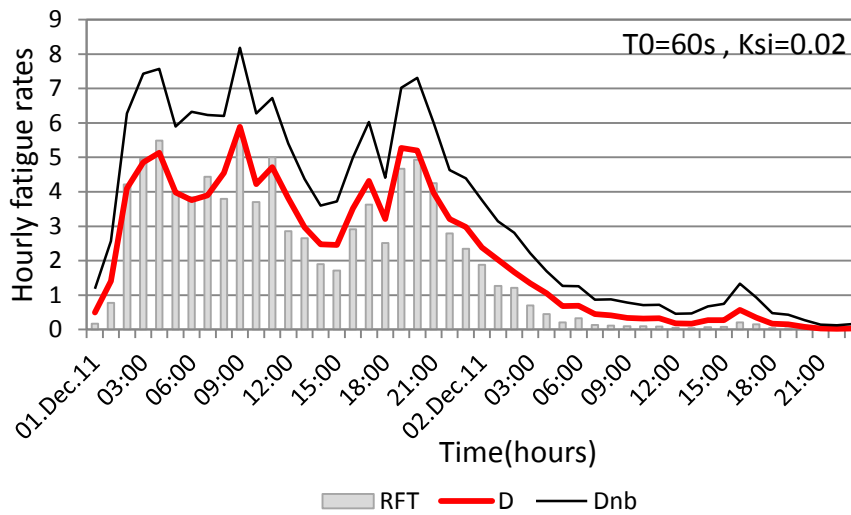


Figure 6.3: The estimated hourly fatigue rates in case 1 (DMP).

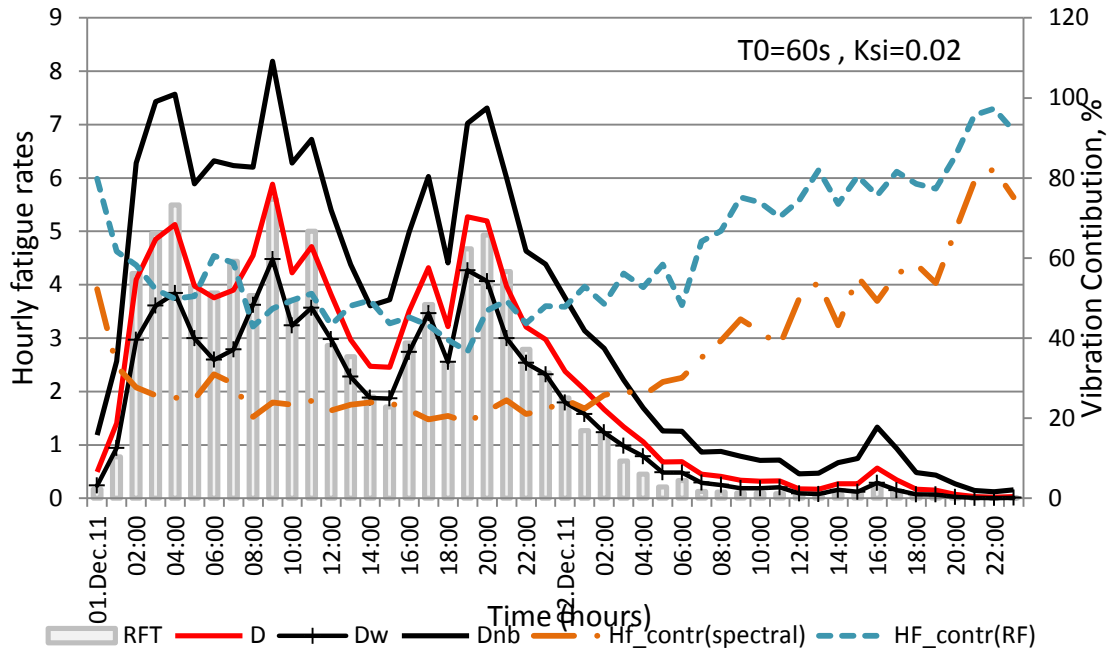


Figure 6.4: The estimated hourly fatigue rates and the vibration contribution in case 1 (DMP)

Case two:

Here the considered period is from 17th November 2010 – 16:00 to 18th November – 23:59. It is the worst encountered storm by the vessels during all the measurements period. Environmental and GPS data are not available during the considered case. The wind sensor was giving unrealistic results and GPS were off or not connected to the hull monitoring system. But it was reported from the ship master that the highest recorded significant wave height H_z was measured in this storm about 5.5 meters, and heading were mainly head seas. The vessel was sailing in the English Channel.

The mean period of the arrival time between each whipping event is estimated graphically from the stress time series as $T_0 = 20s$. And the damping ratio of the vessel is taken as 0.02.

Results of the estimated fatigue rates from narrow banded approximation (Dnb), Jiao and Moan method (D), and Rainflow counting (RFT) are illustrated in figure 6.5. Here high hourly fatigue rates have been recorded, the maximum was at 22:00 17th November. The value of 144 is estimated by Rainflow counting, 100 is estimated by the narrow band approximation and 70 is estimated by Jiao and Moan method. The narrow band approximation is not an upper bound for rainflow anymore, for high stresses Rainflow counting estimates higher fatigue damage then narrow bound approximation and Jiao and

Moan method. Wen fatigue rates are below 20 The Jiao and Moan method is in good agreement with the Rainflow counting.

In figure 6.6, the estimated spectral hourly fatigue rates from the wave responses is presented and high frequency contribution to the total damage as is estimated with both methods, spectral and rainflow counting is illustrated. In this case, the vibration contribution for the both methods increases with the high stresses and decreases when the stress is low. And this is in good agreement with the findings in chapter 5, where the vibration contribution is found to increase with increasing wind strength (B_n), see figure 5.2. In case one, results were different.

It seems that in moderate sea stated (case one) the fatigue damage is mainly caused by vibration.

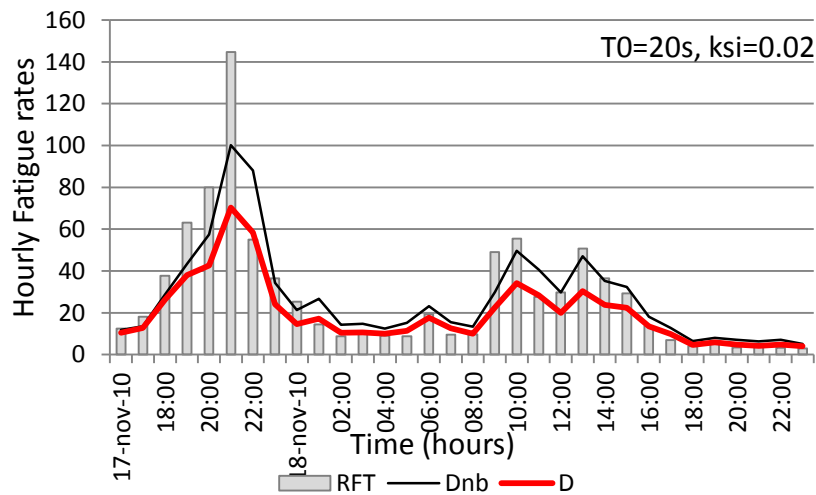


Figure 6.5: The estimated hourly fatigue rates in case 1 (DMP).

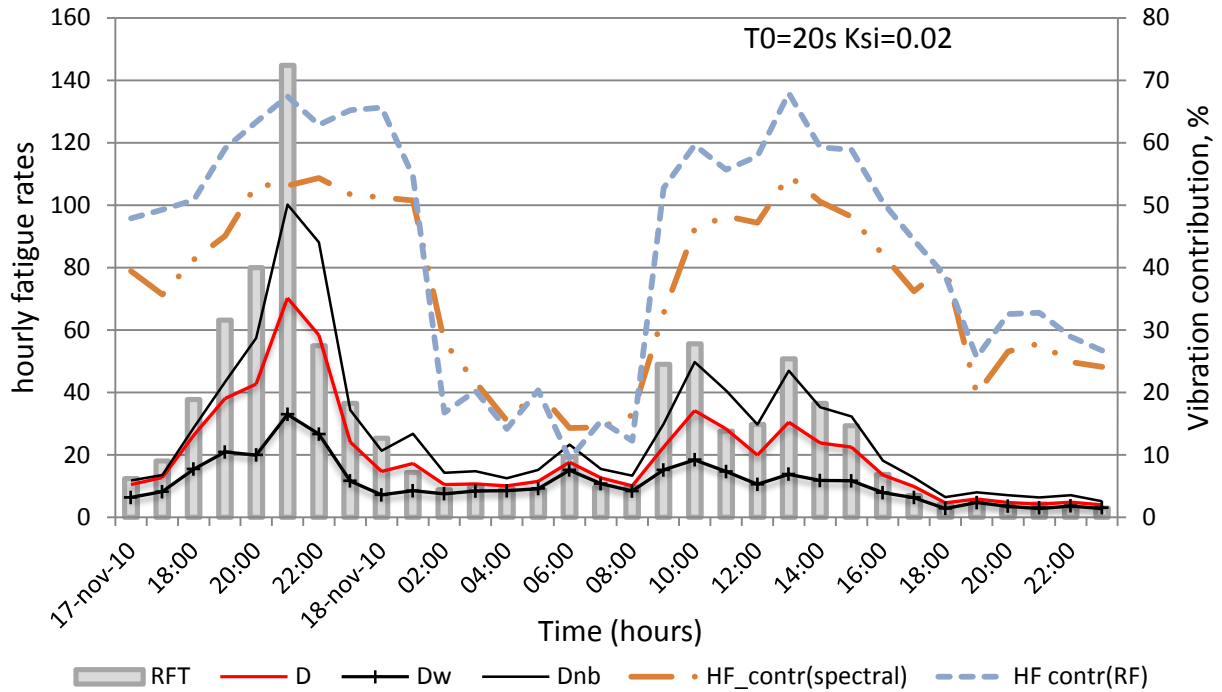


Figure 6.6: The estimated hourly fatigue rates and the vibration contribution in case 1 (DMP)

Linear Springing

In case one, the vessel encountered wind condition of Bn between 3 and 5 and head wind. According to table 5.1 this wind condition corresponds to significant wave height between 1 and 2 meters in head seas. According to eq. 6.8 and wave period may be calculated.

$$T_z = 6H_s^{0.3} \quad (\text{DNV, CN 30.5 2000}) \quad (6.8)$$

T_z is wave period in second and H_s is the significant wave height in meters. By taking the mean significant wave height as 1.5 m the wave period is 6.8 s. and the wave frequency is $\omega_0 = 2\pi/T_z = 0.93 \text{ rad/s}$.

The encountered wave frequency ω_e is calculated from eq. 6.9 (Faltinsen, 1998) having the vessel speed U to be 16knots which is equal to 8.23 m/s, heading angle and β equal to 0 and the gravity acceleration $g = 9.81\text{m/s}^2$

$$\omega_e = \omega_0 + \frac{\omega_0^2}{g} U \cos(\beta) \quad (6.9)$$

This formula gives encountered wave frequency $\omega_e = 1.65 \text{ rad/s}$

And then eq. 6.10 (Faltinsen, 1998) is used to calculate the encountered wave length λ_e .

$$\lambda = \frac{2\pi g}{\omega^2} \quad (6.10)$$

The encountered wave length is $\lambda_e=23\text{m}$, the vessel length $L_{pp}=322\text{ m}$.

About 14 waves are encountered through the ship length, these waves creates linear springing (Faltinsen 1999). In Figure 6.7 the high frequency signal XH is plotted together with the low frequency signal XL. Both stress signals the stress level is low. While for each cycle of XL (wave response) there are about 5 cycles in XH (vibration responses).

This the main reason for the vibration contribution to fatigue damage to be above 90% at the 2nd December 2010 – 23:00

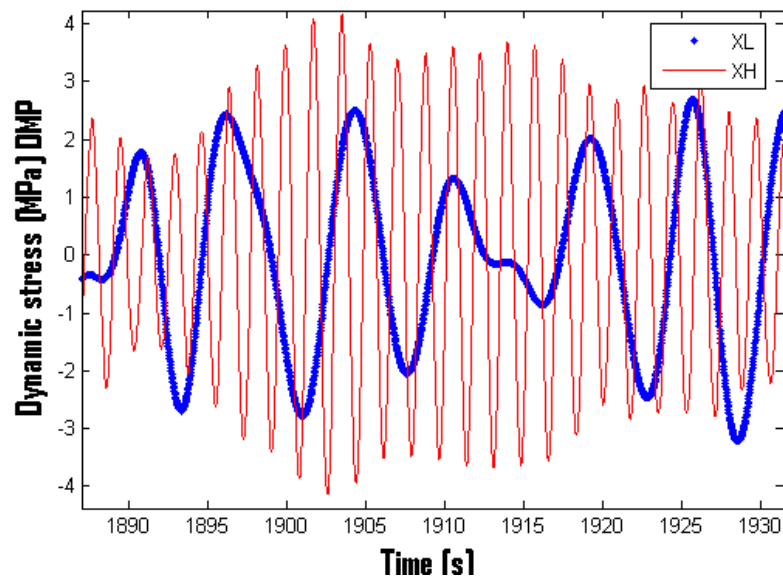


Figure 6.7: linear springing: Low and high frequency stress signals, the 2nd December 2011 –23:00

Discussion

In Jiao and Moan method, the damping ratio ξ and the mean period of the arrival time between each whipping event T_0 have been used. The estimated damage is very sensitive to these two parameters. Then conservatism in estimation of T_0 and ξ will lead to conservatism in the estimated damage.

A spectral method has been used in estimating the damping ratio applied on several times series and gave values for the damping ratio from 0.01 to 0.05. This show that results was not stable.

In both case (case one and case two) the damping ratio was estimated between 0.015 and 0.03. Findings in 4400TEU container vessels gave damping equal to 0.01 (Storhaug et al. 2007).

The vessel considered in this thesis is larger and carrying larger number of container then the damping should be higher than 0.01. According to this 0.02 is judged to be acceptable value for damping.

T_0 is estimated graphically when the stress acceleration increases suddenly. And the chosen values seem to be the most accurate. But that should be verified analytically.

In general, when the stresses are above a certain level, the vibration contribution increase with increasing the stresses (e.g. when the wind strength increases, see chapter 5). But when the stresses are low (at moderate weather conditions), in some cases the vibration contribution increases by decreasing the stress loading, especially when the linear springing is present and the effect of the wave responses tend to zero while the effect of springing become almost the only source for fatigue damage.

In moderate environmental conditions, the estimated damage with Jiao and Moan method provide good agreement with the rainflow damage. While in harsher environmental conditions, the rainflow counting estimates higher fatigue damage then the spectral method. And this difference could be significant (the double in the case of 17th November 2010, 22:00).

Comparing the narrow band approximation method to the Rainflow counting:

-In moderate weather, when the stresses are low, the estimated damage D_{nb} is always higher than the estimated damage with Rainflow method. And this agrees with findings in literature e.g. (Jiao et al. 1990) and (Rychlik, 1993) where the narrow band approximation is considered to be the upper bound for rainflow counting.

-In the other case of harsh weather, the stresses were very high and led to very high fatigue damage. The estimated fatigue damage from Rainflow counting was recorded above the estimated damage from narrow band approximation.

Extreme Loading

For the stress level in deck amidships, the dominating contribution comes from the vertical bending moment, especially at high stress levels. Other components of the stress are axial force, horizontal bending moment and axial warping stresses. In addition, the still water bending will contribute to the overall loading. During the measurement period, the minimum (sagging) and maximum (hogging) dynamic values are determined for each 5 minutes. This is done for both the total signal that included whipping and also for the wave frequency signal, and the results are illustrated in Figs. 20~21 for sensors DMP and DMS, respectively. The stress from the rules wave bending moment from IACS-URS11 is 103MPa in hogging and 127 MPa in sagging (an inaccuracy in reference (Heggelund, et al 2011) states 106 MPa in hogging and 131 MPa in sagging, which may differ depending on how the section modulus is estimated and which drawing revision that has been used). In all the encountered storms the dynamic stress of the wave response signal has been below the IACS rule stress, while this level has been exceeded by the whipping contribution several times both in hogging and sagging. For the DMP sensor the stress was recorded above the rule bending stress in 4 encountered storms, while for the starboard sensor DMS this level has been exceeded in 3 storms. In general, the maximum sagging and maximum hogging are relatively symmetric and they are quite similar for both deck sensors amidships, but port side sensor show higher extreme values than starboard sensor. This may be caused by not pure head sea conditions where other components also contribute. A slight heel may also cause this difference in stress between starboard and port deck stresses. It is observed that the hogging (positive) values are more frequently exceeded than the sagging values, also because the sagging rule values are higher.

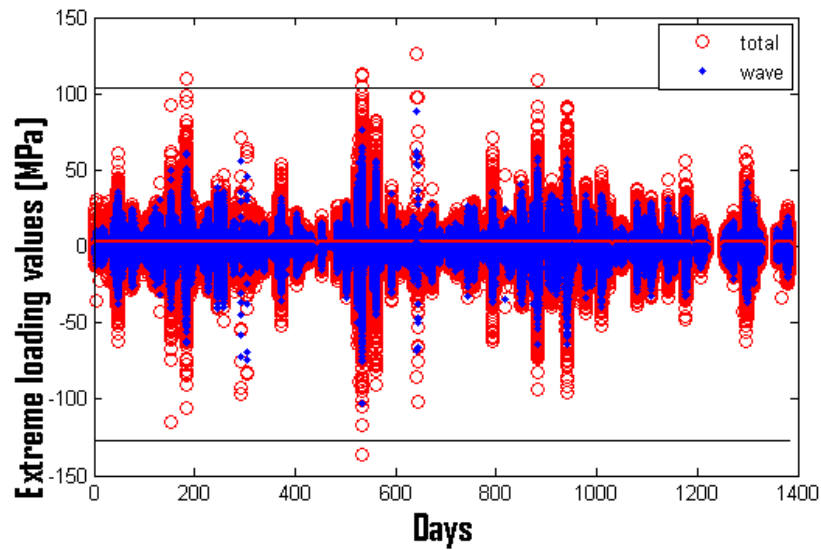


Figure 7.1: The maximum 5 minutes hogging (positive) and sagging stress with and without whipping, DMP.

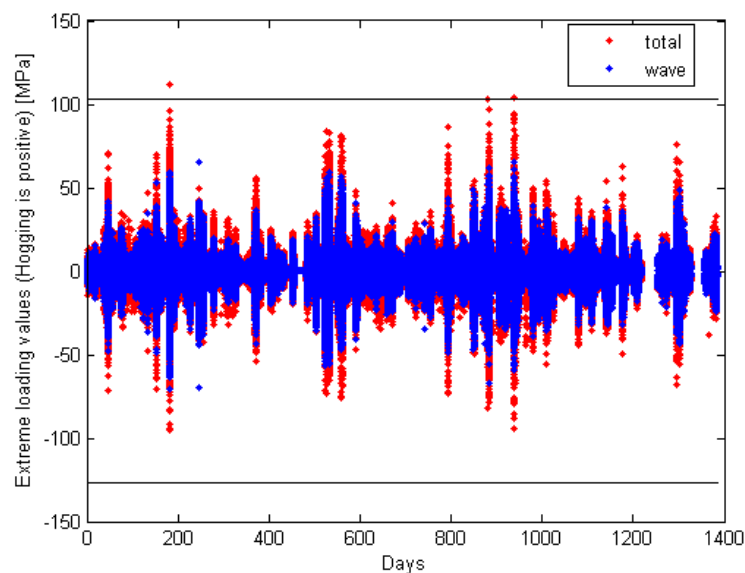


Figure 7.2: The maximum 5 minutes hogging (positive) and sagging stress with and without whipping, DMS.

The highest extreme values with whipping and the highest extreme values without whipping for all the global deck sensors are shown in table 6 based on stress values in MPa. The ratio of those stresses defines the amplification factor due to whipping. The highest extreme values for the total and wave response may however occur in different storms, in the way that extreme loading from wave without whipping may come from a swell like head or stern sea condition while extreme loading when the whipping is significant may come from a steep moderate sea combined with high forward speed in head or bow quartering sea states. The

amplification factors are high and in some cases the dynamic stress is doubled due to whipping. This may easily happen for this vessel with large bow flare and capable of maintaining high speed in harsh sea states. Without proper seamanship and voluntary speed reduction in moderate head sea storms it is possible that the stress level would have been even higher. The extreme values that exceed the IACS rule value are indicated in bold. It occurs in both sagging and hogging for the aft and the midship section, while the forward quarter length section is well below rule values. This is displayed more clearly in Fig. 22, where the maximum extreme loading dynamic stress with and without whipping are divided by the IACS rule wave bending stress. The excess is 48% in hogging aft and 23% in hogging amidships while more than 20% below the rule values in the fore ship. Also maximum sagging is above IACS value by 7% amidships and similarly in the aft ship. It is clear that the hogging values are relatively high, also considering that these will be combined with a still water hog-ging moment in an ultimate capacity check of the hull girder.

The maximum sagging (\min_{dyn}) and hogging (\max_{dyn}) extreme stress from DMP sensor as function of B_n strength and as function of wind headings are illustrated in Figs. 23~24, respectively. The extreme loadings are higher in head and stern seas and decrease in beam seas. The maximum sagging and hogging is actually encountered in stern seas. It should be noted that the wind sensor was not reliable/operational in some of the worst storms, so the worst values are not included in Figs. 23~24. The maximum values also occurred in moderate B_n , suggesting that this are not real wind generated storms but either swell, which are not steep sea states, or moderate sea conditions. The vessel has simply not encountered any really harsh storms yet, but the worst values refer to a sea state of about 5.5m significant wave height, measured by the wave radar onboard. In a North Atlantic trade higher values should be expected. In Fig 23 there is no clear correlation between maximum dynamic stress and B_n strength. The maximum dynamic stress of 126.6 MPa (hogging) has been recorded at the wind condition of B_n 4 and stern wind combined with a forward speed of 20 knots. While for B_n 5 combined with higher forward speed of 21 knots, the maximum dynamic stress was 85 MPa (sagging) in bow quartering. In any case the wind is moderate at it is likely that swell may be the reason for some of these high loadings. It is expected that wave parameters like significant wave height and peak period as well as heading will correlate better with extreme loadings than wind.

Table 7.1:

Maximum sagging and hogging stress with and without whipping and the IACS wave bending stress rule

Location		L/4	L/2	3L/4			
Sensor		DAP	DAS	DMP	DMS	DFP	DFS
Hogging	Total	108	94,4	126,6	111,8	70,7	60,2
	wave	52,9	49,9	88,6	65,4	46,8	36,6
	IACS	73,0	73,0	103,2	103,2	101,4	101,4
	F _{amplification}	2,1	1,9	1,4	1,7	1,5	1,6
	Total	-99	-116	-136,4	-95,5	-96,4	-99,6
Sagging	Wave	-59	-59	-102	-70,5	-59,4	-51,3
	IACS	-90	-90	-127,1	-127	-125	-125
	F _{amplification}	1,7	2,0	1,3	1,4	1,6	1,9

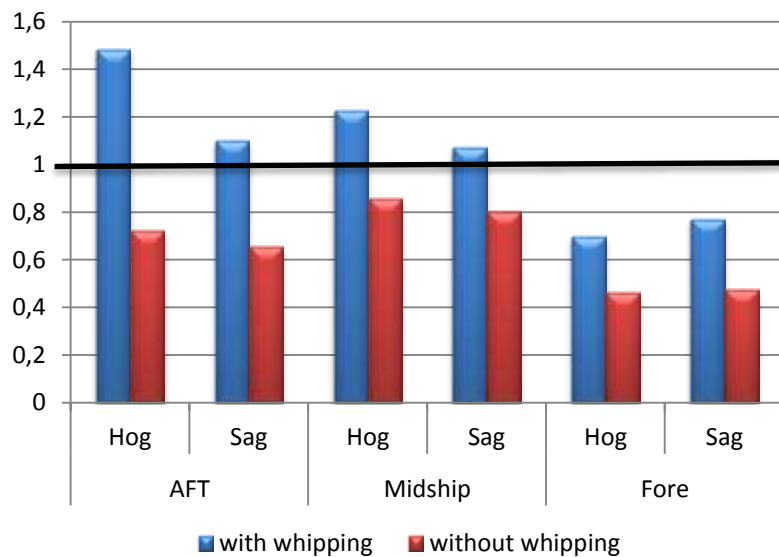


Figure 7.3: The Measured Stress versus IACS Rule stress from port side sensors.

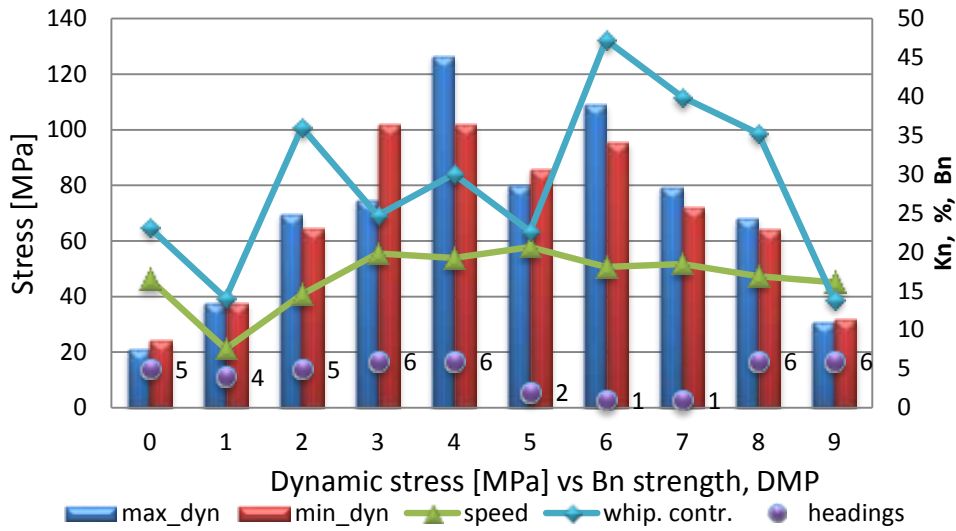


Figure 7.4: The Extreme dynamic loading versus wind strength for DMP.

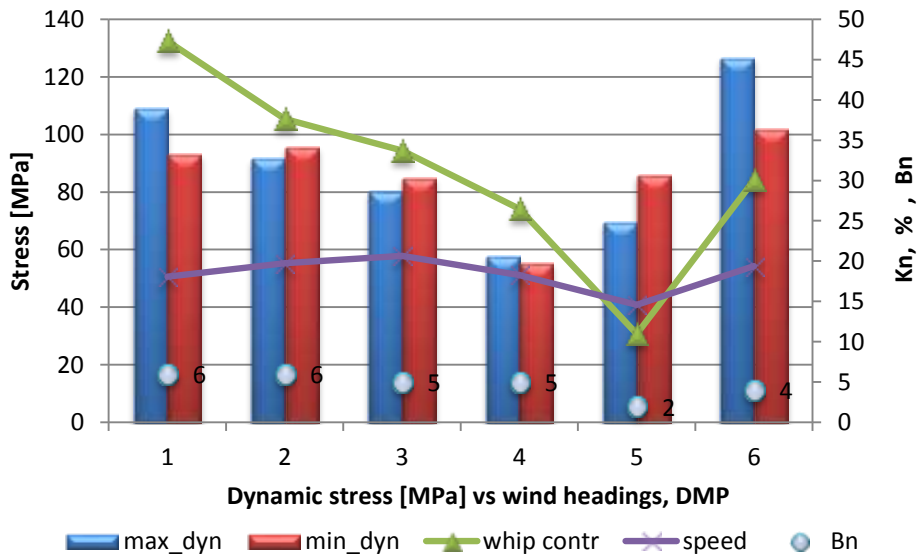


Figure 7.5: The Extreme dynamic loading versus wind headings for DMP.

Chapter 8**Summary and Conclusions****Major Findings and Discussion**

An 8600 TEU container vessel has been investigated. It has been sailing in East Asia to Europe trade. Measurements have been collected from about 4 year's period, 27% of the time the vessel was in port area. 20 voyages from North Europe to East Asia and back have been performed in a regular pattern. The average time spent in each voyage is 70 days.

The data assessed in this thesis are mainly recorded from the stress sensors for global responses in deck, the wind sensor and the GPS. The total effective measurements recorded by the hull monitoring system and stored in the statistical data covers 3.7 years. The wind sensor has not been always reliable. Therefore, the effective wind data covers only 2.7 years. The measured wind profile suggests that Bn (Beaufort strength) of 3 is most frequent. The true heading profile suggest prevailing wind conditions from northern and north eastern direction, while head and stern seas dominates slightly the encountered wind direction on this trade. The position plot confirms that routing to avoid storms is not carried out even though voluntary speed reduction is observed.

The estimated fatigue life from the measurements is 49 years based on a corrosive SN-curve and a stress concentration factor of 2. Even though the vibration contributes to about 57% of the fatigue damage amidships, fatigue is not regarded as an issue for this trade and vessel. The vessel has encountered low wind strength conditions compared to the North Atlantic. 95% of the time at sea, the encountered wind strength was below 5 Bn with average 5 minutes damage to be 11% of the design budget damage. The maximum fatigue rates even in this "calm" trade has been record high and exceeds what has been experienced as maximum fatigue rates on Panamax container vessel in North Atlantic, five minutes fatigue rate of 373 have been recorded in deck amidships. . It can therefore not be concluded that fatigue for this vessel would not have been an issue if this vessel is trading regularly in North Atlantic trade. This trade is not so relevant for this Post Panamax size today, but may become relevant in the future.

From the fatigue assessment it is clear that most of the fatigue damage comes from head to beam seas, (46% of the time give 74% of the total damage), while beam to stern seas give minor contribution (26% of the total damage). Bow quartering is the worst heading, (29% of the total damage with 0.5 average five fatigue rate), possibly due to the wave being effectively longer compared to this large vessel. The relative vibration contribution is large and decays from 64% in bow quartering to 39% in stern seas, it is still significant in stern seas. Findings from smaller container vessels (Storhaug 2011) show also significant vibration contribution in stern seas (24% in 2800TEU and 19% in 4400TEU) and it increases from head to stern seas but slower than in the current vessel.

According the results the wind headings may be divided into 3 groups:

Head and bow quartering, are the worst headings, contributes by 58% to the total fatigue damage, with 36% encounter probability. Bn 6 contributes to most of the fatigue damage. and the average speed tends to reduce by increasing Bn. The average fatigue rates and the vibration damage contribution increase with Bn. Head sea is more frequent than bow quartering. While the latest is more critical assuming an even encountered heading profile. Results from these sectors agree quite good with results from other smaller vessels (Storhaug 2012). Where Bn 6 also contributes to most of the fatigue damage, the vibration contribution increases with increasing Bn, but slower than in the current vessel. In the 4400TEU container vessel the average damage also increase with Bn such as in the considered vessel. In the smaller container ships head sea are more critical then bow quartering with is not the case for this large vessel, this is may be due the length of the vessel ($Loa = 340$ m) encountering small seas states, so the wave length appears longer, and then quartering seas give higher significant wave bending moment.

In Beam seas (sector 3, 4 and 5), the total probability of encounter is 33% and contributes by 28% to the total fatigue damage. Bn 5 contributes most the fatigue damage. The average fatigue rates are very low until Bn 4 and then increases significantly higher Beaufort numbers. The vibration contribution also increases with increasing Bn. The average vessel's speed increases with increasing Bn for sector 3, while it remains constant or decrease slightly for the other two sectors.

In Stern seas, the probability of encounter is 31% while it contributes by only 15 % to the total damage. The vibration contribution is also high in stern seas but it does not show a clear trend by increasing Bn. Bn 4 is the most contributing. The average damage is low even for Bn

up to 7. The vessel speed increase slightly by increasing Bn. Findings from the smaller report also that the average fatigue rate and average speed increase by increasing Bn. While Bn 5 contributes most to fatigue damage in stern sea and the vibration contributes decreases by increasing Bn (in 4400TEU). Bn 5 contributes most to the fatigue damage.

The rainflow counting estimate higher values for the vibration contribution than the spectral method of Jiao and Moan. At high stresses, both methods show that the vibration contribution tends to increase with increasing stresses. Knowing that trends from those periods with high stresses effect the general trends of the whole measurements period regarding fatigue damage. In some cases with low stress, when the vessel encounter short wave from head seas, the linear springing may contributes more to fatigue damage, and by reducing the stresses the contribution on the waves responses tend to zero, therefor the vibration contribution increases with decreasing the stresses.

The narrow band approximation can be considered upper bound for the rainflow counting only when there is no high contribution from whipping.

When the stress levels are moderate, the spectral method provides good agreement with the Rainflow counting in estimating the fatigue damage. While severe weather condition, the spectral method estimated lower fatigue damage, in extreme cases it estimates only half of the damage estimated by the Rainflow counting. When high whipping is present the damage estimated by the rainflow counting exceeds even the damage estimated by the narrow band approximation.

And here the question is: Does the general consensus of “the Rainflow counting technique provides the most accurate estimate for the fatigue damage” is always valid? Even though when there are high frequency response (whipping) superposed to high wave response? Some research shows that this is not correct (Gotoh et al. 2012). The validity of this assumption has to be more investigated.

The whipping contributes significantly to increase the dynamic extreme stresses in deck, doubling the dynamic extreme stress in both hogging and sagging at aft quarter length. The effect of whipping can also be considerable amid-ships and at forward quarter length. With whipping the total dynamic stress exceeds the IACS rule in both sagging and hogging at aft quarter length and amidships. The exceedance has been up to 48 % in hogging at aft quarter length, corresponding to where MSC Napoli broke in two. In the forward quarter length the

IACS rule stress has not been exceeded, and the wave frequency stress has not in any cases exceeded the IACS rule stress. The vessel has not encountered any real severe storms yet, only up to 5.5m significant wave height for the highest measured stress so far, but the extreme measured values have been encountered in moderate/small storms but at high speed. All of this agrees fairly well with observations of the same vessel in model tests. The extreme loading values do not correlate well with the wind strength since it appears that swell may affect the measured extreme stress in the various headings. For this correlation it would have been better to use wave heights and wave periods, but for the fatigue the wind sensor tends to provide useful data.

Given that the contribution of whipping is high both in fatigue and extreme loading, good seamanship is considered useful even though routing appears less relevant in this trade. This seamanship may become more significant on these large container vessels with high bow flare angle and capable of maintaining high speed in harsh head sea storms simply because the tall superstructure will make it uncomfortable on the bridge when exposed to high acceleration levels in all three directions due to high whipping events. This factor may be important in development of ship design rules when whipping should be included explicitly on container vessels. Neglecting realistic assumptions in sea states, routing and seamanship may result in too conservative guidelines.

The hull monitoring system was running and providing valuable measurements most of the time. However, in some sensors some unrealistic peaks have been recorded in the stress signal. Then some procedures were necessary to clean the statistical data related to the stress such as fatigue rates and dynamic loadings. About 10 % of data was removed.

Because of the problem of the wind sensors, wind measurements of 1.5 years have been considered bad. And this would not happen if the problem were detected earlier. This problem cannot be counted cons for the hull monitoring system. However user should have better contact with the system, in order to detect any problem, e.g. in the installation manual the loading computer should be connected to the hull monitoring system, however, there were no records related to loading computer in the stored data.

Although, the hull monitoring system still providing important real time display for: wind and wave velocities, pitch, roll, accelerations, bow pressure, deck stress, course, speed, and slamming events, alarm warning about high fatigue rates and extreme loadings. A lot of valuable information can be used as the basis for making decision. It can be used by the crew on

board e.g. to avoid storms. And it is also basis for making decision on shore by defining acceptance basis for acceptance criteria in design. The stored data represent big inspiration for researcher to reveals physics which are not considered in the design and for further development of the numerical codes.

Future Work

Only few number sensors have been used to produce the results in this thesis. However, many other sensors are available and may be used for producing more findings and results.

Container vessels are characterized by the large hatch opening, Due to this structural property, they are subject to large diagonal deformations of hatch openings and warping stresses under complex torsional moments in waves. This necessitates torsion strength assessment of hull girders in container ships at their structural design stage, which is not well clarified in the main classification rules. The torsion stress becomes increasingly important, especially in the areas of transversal stiff structures. 4 sensors are available at the transverse deck strip and may be used for estimating the torsion induced responses and specific sea states. How the wave/wind conditions effect influence the Torsion? Does the Torsion contribute to fatigue loading?

In Gotoh (2012), was reported that the traditional fatigue life estimation procedures based on the S-N curves approach with Rainflow counting combined with Palmgren-Miner rule is inappropriate and overestimate the fatigue damage when significant whipping is superposed to the wave responses. And this is the case for the considered large container vessel. Gotoh et al. propose a numerical simulation based on advanced fracture mechanics to estimate the fatigue crack propagation under superposed loading condition with low and high frequency. And new cycle counting procedures were used.

Does the proposed method applicable for estimation the fatigue damage using the available stress time series from the container vessels?

References

- Almar Næss, A. (1985). *Fatigue Handbook, Offshore structures*. Trondheim: Tapir Publishers.
- ASTM. (1997). Standard practices for cycle counting in fatigue analysis, Annual Book of ASTM Standards. Vol 03.01, designation E1049-85. *ASTM* , 693-701.
- ASTM. (2005). *Standard Practices for Cycle Counting in Fatigue Analysis*. ASTM International.
- Barsom, J. M. (1976). Fatigue crack growth under variable amplitude loading in various bridge steels. *Fatigue crack growth under spectrum loads ASTM* , 217-237.
- Benasciutti, D., & Tovo, R. (2007). On fatigue damage assessment in bimodal random processes. *International Journal of Fatigue* , Vol. 29, pp.232-244.
- Bendat, J. S. (1964). *Probability functions for random responses: Predictions of peaks, fatigue damage and catastrophic failures*. NASA.
- Bengtsson, A., Bogsjö, K., & Rychlik, I. (2009). Uncertainty of estimated rainflow damage for random loads. . *Marine Structures* , , Vol. 22, pp. 261-274.
- Bengtsson, A., & Rychlik, I. (2009). Uncertainty in fatigue life prediction of structures subject to Gaussian loads. *Probabilistic Engineering Mechanics* , Vol. 24, pp. 224-235.
- Berge, S. (1981). Analysis of the fatigue failure of the “Alexander L, Kielland”. *American Society of Mechanical engineers (ASME)* .
- Cargo Law*. (2007). Retrieved from Cargo Law:
http://www.cargolaw.com/2007nightmare_msc.napoli4.html
- DNV. (.April, 2007.). *Environmental conditions and environmental loads, Recommended Practice*.
- DNV. (2010). Fatigue Assessment of Ship structures . *DNV Classification Note No. 30.7* , .
- DNV-RP. (2010). *RISER FATIGUE*.
- Dowling, N. E. (2004). Mean Stress Effects in Stress-Life and Strain-Life Fatigue. *Fatigue 2004: Second SAE Brazil International Conference on Fatigue*,. São Paulo, Brazil.
- Faltinsen, O. M. (1998). *Sea Loads on Ships and Offshore Structures*. Cambridge UK: Cambridge University Press.
- Fatemi, A., & Yang, L. (1998). Cumulative fatigue damage and life prediction theories: a survey of the state of the art for homogeneous materials. *J Fatigue* , Vol. 20 (1), pp. 9-34.
- Fatigue crack growth under variable-amplitude loading in various bridge steels, Fatigue Crack Growth Under Spectrum Loads,. (1976). *ASTM STP 595 American Society for Testing and Materials* , pp. 217–235.
- Fleet Mon*. (2012). Retrieved from
http://www.fleetmon.com/en/vessels/Hyundai_Global_61570/photos
- Gao, Z., & Moan, T. (2007). Fatigue Damage Induced by non Gaussian Bimodal Wave Loading in Mooring Lines. *Applied Ocean Research* , Vol. 29, pp. 45-54.
- Goodman, J. (1919). *Mechanics Applied to Engineering*. Longmans,. *Green and Co. London* , pp. 631-636.

- Gotoh, k., Matsuda, K., & Kitamura, O. (2012). Numerical simulation of fatigue crack propagation under superposed loading histories with two different frequencies. *Hydroelasticity in Marine Technology*. Tokyo Japan.
- Gotoh, K., Toyosada, M., & Niwa, T. (2003). Fatigue crack propagation for a through thickness crack: a crack propagation law considering cyclic plasticity near the crack tip. *International Journal of Fatigue* , Vol 26, PP 983-992.
- Heggelund, S. E., Storhaug, G., & Choi, B. K. (2011). Full scale measurements of fatigue and extreme loading including whipping on an 8600TEU Post Panamax Container vessel in Asia to Europe trade. *OMAE*. Rotterdam Holland.
- Hermundstad. (2007). *Springing and whipping of ships lecture notes Lecture notes in Hydroelasticity*. MARINTEK / CeSOS.
- holm, S., & Mare, J. (1988). A simple model for fatigue life. *IEEE Trans. Reliab.* , Vol. 37, pp.314-322.
- IACS. (2006). Common Structure Rule for Bulk Carriers (Common Structure Rule for Oil Tanker).
- IACS. (2010). *Longitudinal strength atandard, Unified Requirements concerning strength of ships S11, Rev. 7. 2010*.
- IMO, & Centre, M. K. (2012). *International Shipping Facts and Figures –Information Resources on Trade, Safety, Security, Environment*.
- Jiao, G., & Moan, T. (1990). Probabilistic analysis of fatigue due to Gaussian load processes. *Probabilistic Engineering Mechanics* , Vol. 5, pp.76-83.
- Johannesson, P., Svensson, T., & De Mare, J. (2005). Fatigue life prediction based on variable amplitude tests – methodology. *International Journal of Fatigue* , Vol. 27,pp. 954–965.
- Matsuishi, M., & Endo, T. (1968). Fatigue of Metals Subjected to Varying Stress. *Proceedings of the Kyushu Branch of Japan Society of Mechanics Engineering*,. Fukuoka, Japan.
- Miner, M. A. (1945). Cumulative damage in fatigue. *Journal of Applied Mechanics* , Vol. 12, pp. 159-164.
- Miyahara, K., Miyake, R., Abe, N., Kumano, M., & Nakajima, Y. (2006). Full-scale measurements on hull response of a large container ship in service. *25th OMAE*. Hamburg, Germany: ASME.
- Moe, E., Holtmark, G., & Storhaug, G. (2005). Full scale measurements of the wave induced hull girder vibrations of an ore carrier trading in the North Atlantic. *RINA, International Conference, Design and Operation of bulk carriers*, (pp. 57-85). London, UK.
- Okada, T., Takeda, Y., & <aeda, T. (2006). On board measurement of stresses and deflections of a Post-Panmax containership and its feedback to rational design. *Marine Structures* , 19:141–72.
- Olagnon, M., & Guédé, Z. (2008). Rainflow fatigue analysis for loads with multimodal power spectral densities. *Marine Structures* , Vol. 21(2-3),pp.160-176.
- Palmgren, A. (1924). Die lebensdauer von kugellagern. *Verfahrenstechnik* , pp339-341.
- Pear Drop*. (n.d.). Retrieved from <http://www.pear-drop.co.uk/beaufort.htm>
- Rychlik, I. (1993). On the —narrow-band|| approximation for expected fatigue damage. *Probabilistic Engineering Mechanics* , Vol. 8, pp. 1-4.

- Sakai, S., & Okamura, H. (1995). On the Distribution of Rainflow Range for Gaussian Random Processes with Bimodal PSD. *JSME International Journal Series A. mechanics and material engineering.* , Vol. 38-A. pp.440-445.
- Schijve, J. (1963). The Analysis of Random Load Time Histories With Relation to Fatigue Tests and Life Calculations. *Fatigue of Aircraft Structures, McMillen* , pp. 115-149.
- Smith, K. N., Watson, P., & Topper, T. H. (1970). A Stress-Strain Function for the Fatigue of Metals. *ASTM Journal of Materials* , Vol. 5 (4), pp. 767-778.
- Storhaug, G. (2007). *Experimental investigation of wave induced vibrations and their effect on the fatigue loading of ships*. Trondheim: Tapir Uttrykk.
- Storhaug, G. (2009). THE 4400TEU CONTAINER VESSEL MSC NAPOLI BROKE IT BACK, BUT DID WHIPPING CONTRIBUTE? *Hydroelasticity in Marine Technology*. niversity of Southampton, UK.
- Storhaug, G. (2012). The effect of heading on springing and whipping induced fatigue damage measured on container vessels. *The 6th International Conference on Hydroelasticity in Marine Technology* . Tokyo Japan.
- Storhaug, G., Choi, B. K., Moan, T., & Hermundstad, O. A. (2010). Consequence of whipping and springing on fatigue for a 8600TEU container vessel in different trades based on model tests. *PRADS2010*. COPPE, Brazil.
- Storhaug, G., Moe, E., & Piedras Lopes, T. A. (2007). Whipping Measurements Onboard a Midsize Container Vessel Operating in the North Atlantic. *Proceedings (RINA, CMP and SNAME), International Symposium on Ship Design and Construction*, (pp. pp. 55-70.). Shanghai, China,.
- Storhaug, G., Pettersen, T., Oma, N., & Blomberg, B. (2012). The effect of wave induced vibrations on fatigue loading and the safety margin against collapse on tow LNG vessels. *The 6th International Conference on Hydroelasticity in Marine Technology* , (pp. 355-365). Tokyo Japan.
- Storhaug, G., Vidic-Perunovic, J., Rudinger, F., Holtsmark, G., Helmers, J. B., & Gu, X. (2003). Springing/whipping response of a large ocean going vessel- A comparison between numerical simulations and full scale measurements. *3rd international conference on Hydroelasticity in Marine Technology*, (pp. 117-131). Oxford UK.
- Taheri, F., Trask, D., & Pegg, N. (2003). Experimental and analytical investigation of fatigue characteristics of 350WT steel under constant and variable amplitude loadng. *Marine Structures* , Vol. 16 (1), pp. 69-91.
- Tovo, r. (2002). Cycle distribution and fatigue damage under broad-band random loading. *International Journal of Fatigue* , Vol. 24, pp.1137-1147.
- Toyosada, M., Yamaguchi, K., Niwa, T., Takenaka, H., Kajumoto, K., & Yajima, H. (1991). Proposal for new parameter for fatigue crack propagation rate based upon the compliance changing phenomena and the developement of its measuring method. *Journal of Society of Naval Architects of Japan* , Vol 55: PP 169:245.
- Van Dyk, J. M. (1981). Envelopes of broad band process,. *M. Sc. Thesis, Det. of Civil Engineering, MIT* , . Cambridge.
- Van Paegpegem, W., & Degrieck, J. (2002). Effects of load sequence and block loading on the fatigue response of fiber-reinforced composites. *Mechanics of Advance Material and Structure* , Vol. 9 (1), pp. 19-35.

Watson , P., & Dabell , B. J. (1975). *Cycle counting and fatigue damage symposium on statistical Science aspects of fatigue testing*. Warnick University.

Appendix A

Sensor Names and Locations

Overview of location of strain sensors:

Amidships between frame 101 and 102

4 sensors in port side (DMP, ISP, SFP, SWP)

4 sensors on starboard side (DMS, ISS, SFS, SWS)

(D=deck, M=midship, IS=Inner side, SF=Side flange, SW=Side web)

(Last letter: P=port, S=Starboard)

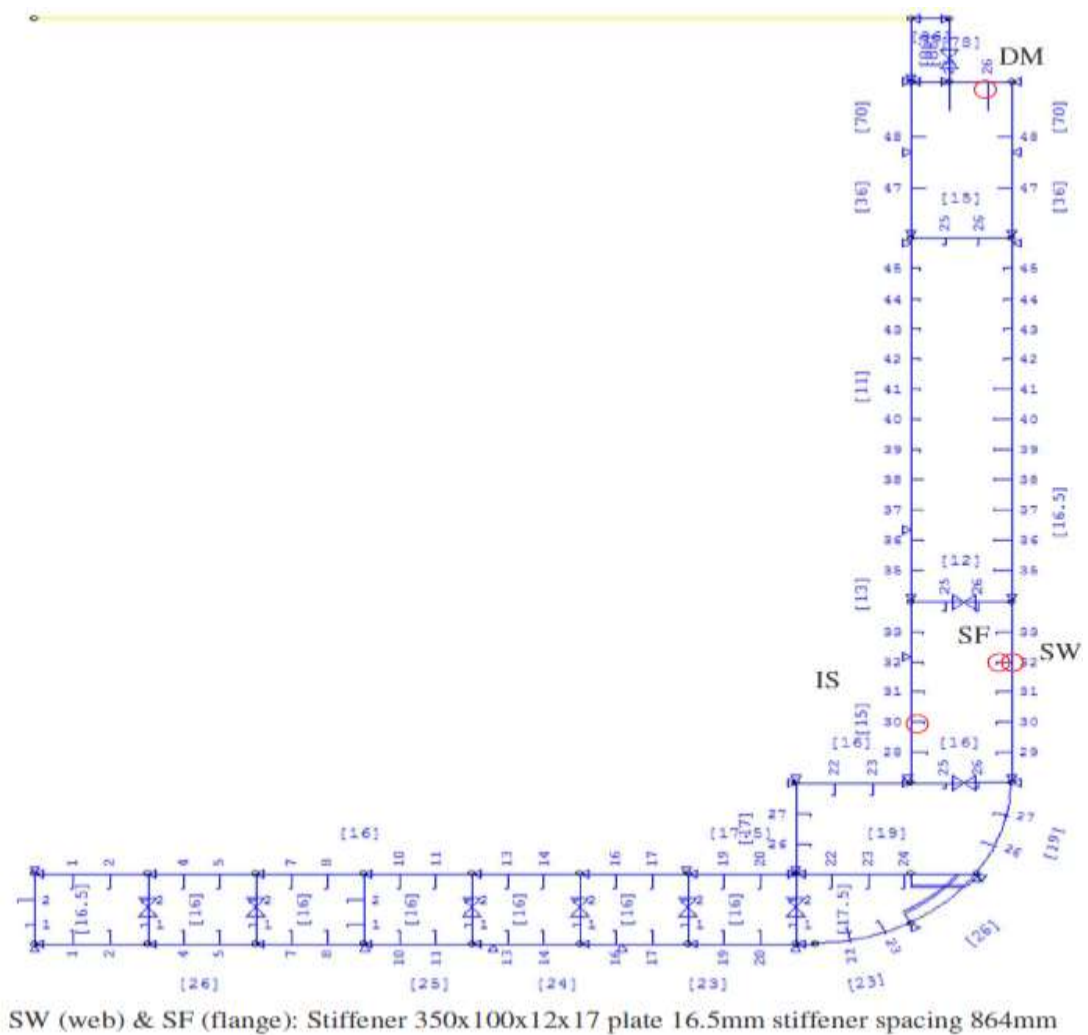


Figure A.1: Amidships sensor positions.

SW: Located at moment zero point for local bending, and at neutral axis of stiffener plate configuration, on upper side of stiffener

SF: Located on midspan, on upper side of stiffener, close to flange

IS: Located at moment zero point for local bending, and at neutral axis of stiffener plate configuration, on upper side of stiffener

DM: Located at “moment zero point for local bending”, and at “neutral axis of stiffener plate configuration”. On outer side of stiffener web

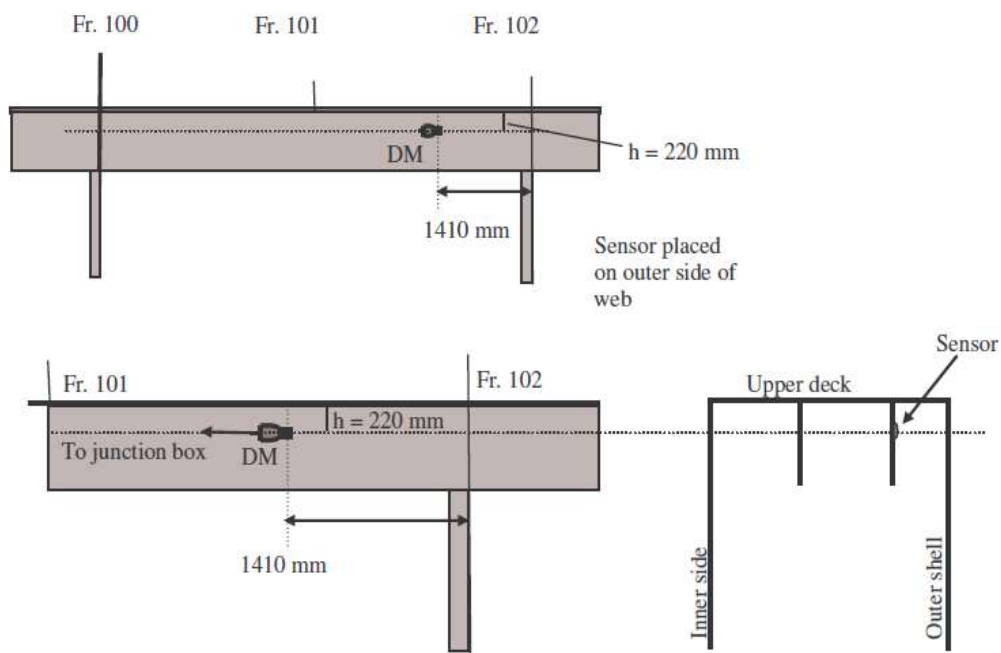


Figure A.2: Position of sensor on deck longitudinal midship (DM).

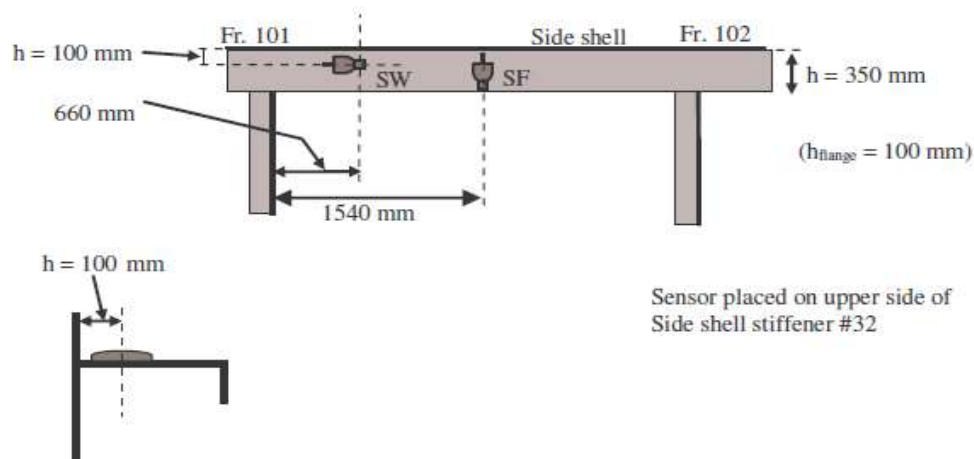


Figure A.3: Position of sensors on side longitudinal (SW and SF)

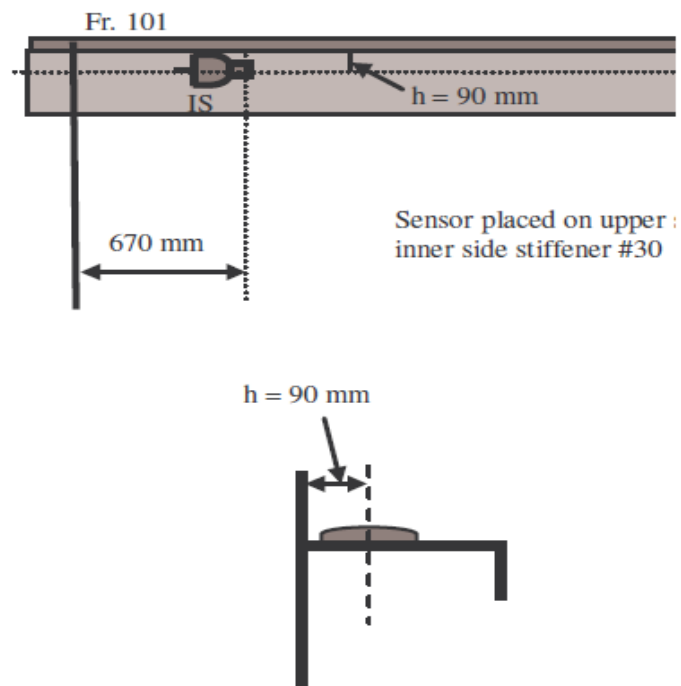


Figure A.4: Position of sensor on inner side longitudinal (IS)

At engine room bulkhead between frame 79 and frame 80

1 sensor at deck on port side (DAP) (D=deck, A=aft, P=port)

1 sensor at deck on starboard side (DAS) (D=deck, A=aft, S=starboard)

1 sensor on port side (IAP) (I=inner side, A=aft, P=port)

1 sensor on port side (IAS) (I=inner side, A=aft, S=port)

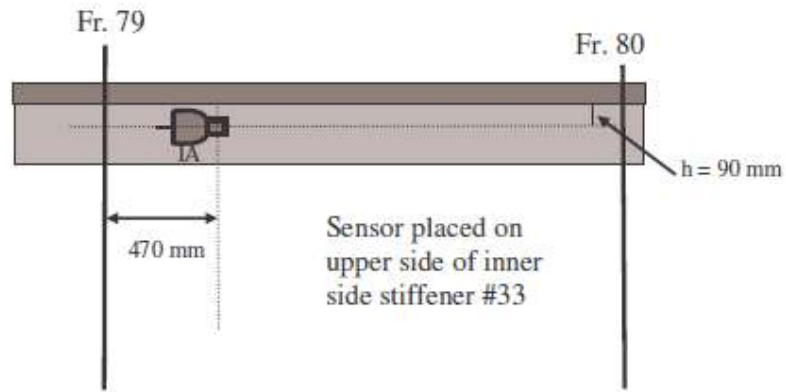


Figure A.6: Position of sensor on inner side longitudinal aft (IA)

At forward quarter length between frame 131 and frame 132

1 sensor on port side (DFP) (D=deck, F=Forward, P=port)

1 sensor on starboard side (DFS) (D=deck, F=Forward, S=starboard)

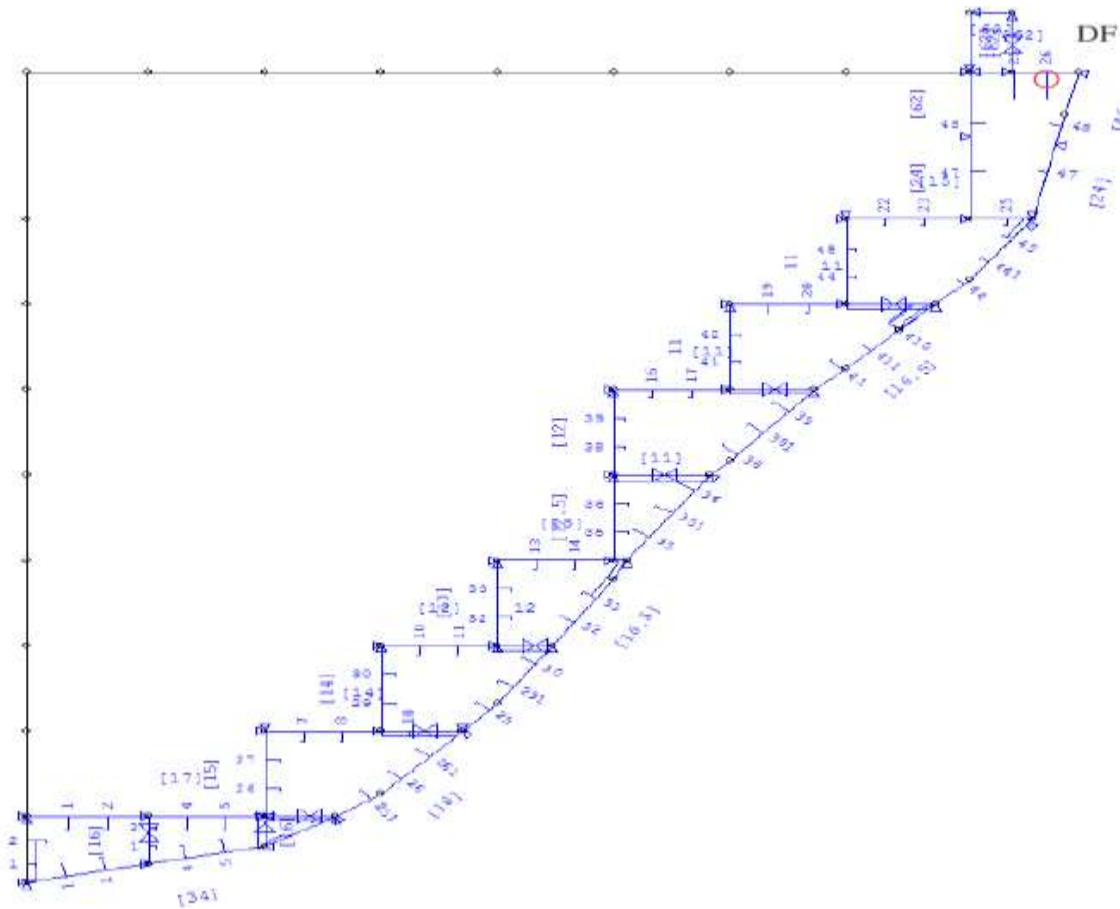


Figure A.7: Forward sensor position.

DF: Located 1.08m forward of frame 131, and at “neutral axis of stiffener plate configuration”, on outer side of stiffener web. No problem with exact location, because no lateral bending.

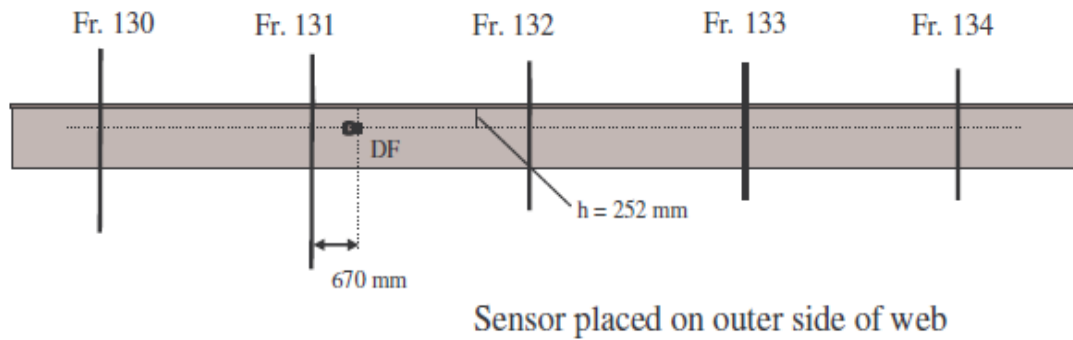


Figure A.8: Position of sensor on deck longitudinal forward (DF)

Note: All figure and sensor details in this appendix are from: *Hull Stress Monitoring System on HHI 8600 TEU container ship - Overview of location of strain sensors.* (LS)

At transverse deck strip:

The sensors are placed at the start of the rounded corner between the deck strip and the side as close to the frame/ bulkheads as possible.

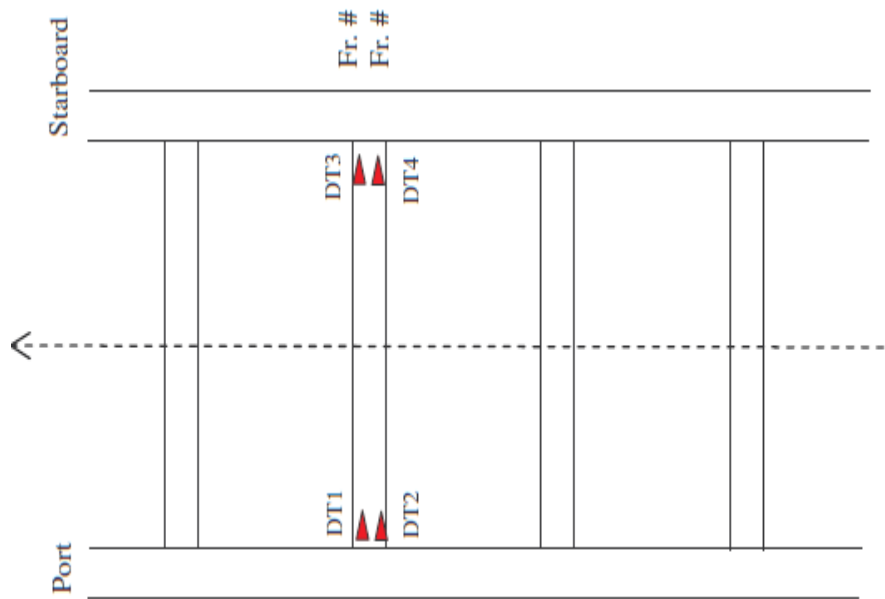


Figure A.9: sensor position at transverse deck strip.

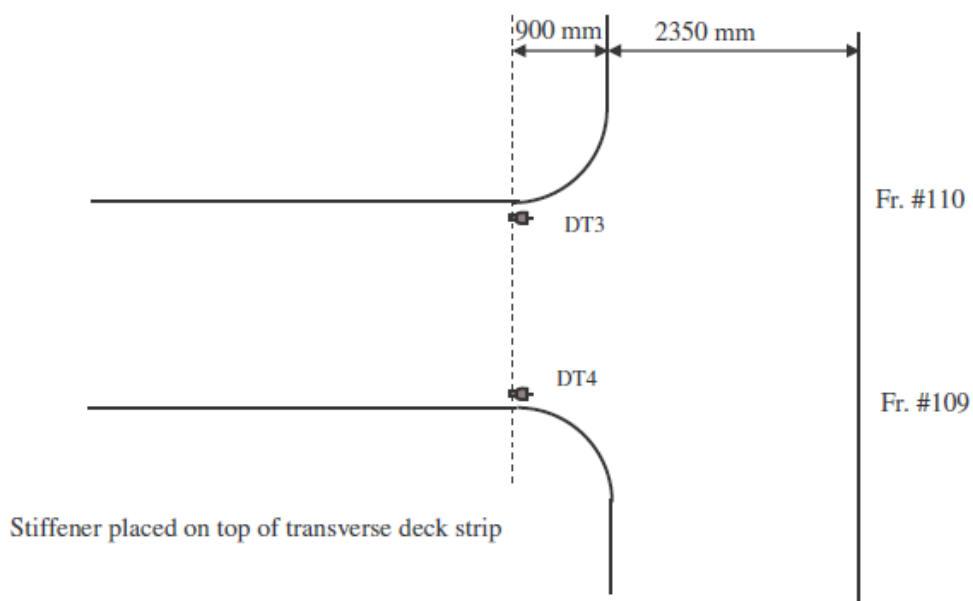


Figure A.10: Position of sensors on transverse deck strip (DT1 – DT4)

Slamming sensors:

2 slamming sensors in double bottom forward and aft (SLF, SLA) to detect the vertical motion due to sea conditions at the center line of the flare.

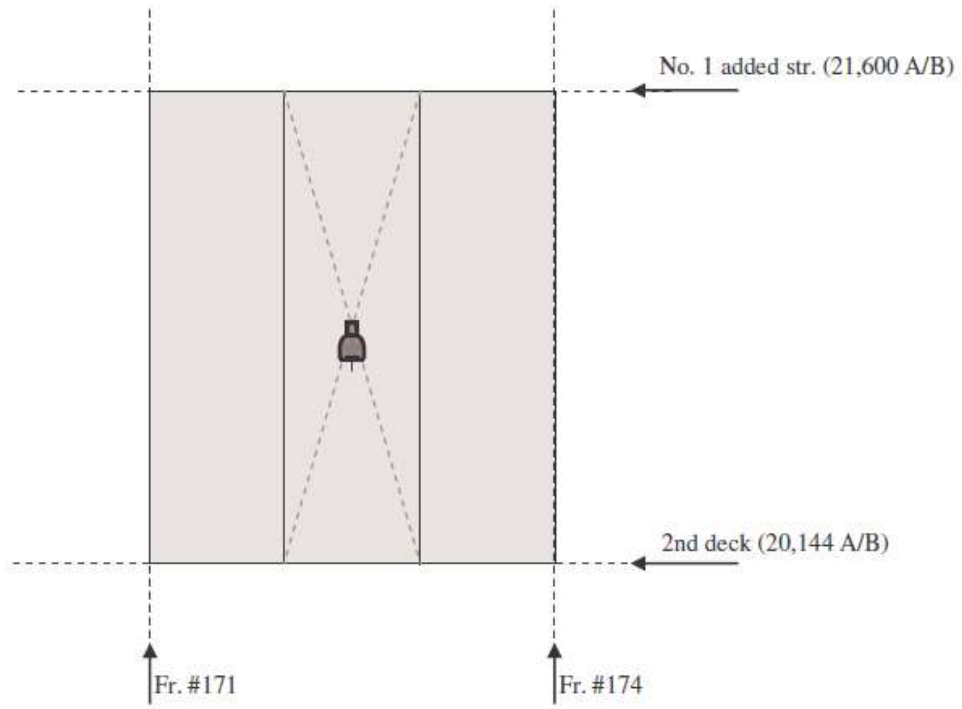


Figure A.11 : Position of forward slamming sensor (SLF)

Appendix B

Research Paper